energies

Article

Supplementary Materials for the work titled "Laminar Natural Convection in a Square Cavity with a Horizontal Fin on the Heated Wall: A Numerical Study of Fin Position and Thermal Conductivity Effects"

Saleh A. Bawazeer

Department of Mechanical Engineering, College of Engineering and Architecture, Umm Al-Qura University, Makkah 21955, Saudi Arabia

The natural convection problem is influenced by the Rayleigh number (Ra), Prandtl number (Pr), conductivity ratio (k_{fin}/k), fin length (L_{fin}), fin thickness (W_{fin}), and fin position (Y_{fin}). A parametric study is conducted by varying these parameters to investigate their effects on heat transfer and flow behavior within the enclosure. The specific ranges considered for each parameter are summarized in **Table S1**.

Table S1. Range of Investigated Parameters.

Parameter	Values	Notes
Rayleigh Number (Ra)	10, 10^2, 10^3, 10^4, 10^5, 10^6	Defines buoyancy-driven flow strength
Prandtl Number (Pr)	0.1, 0.5, 0.71, 1, 5, 10	Influences thermal diffusivity
Conductivity Ratio (k_{fin}/k)	1, 10, 10^2	Accounts for fin material effect
Fin Length (L_{fin})	0.1, 0.3, 0.5, 0.7, 0.9	Defines horizontal length
Fin Thickness (W_{fin})	1×10^{-3}, 1×10^{-2}, 1×10^{-1}	Affects conduction and flow blockage, influences heat transfer efficiency
Fin Position (Y_{fin})	0.1, 0.3, 0.5, 0.7, 0.9	Defines vertical placement
Base Case	$Pr = 0.71$, $k_{fin}/k = 1$, $L_{fin} = 0.5$, $Y_{fin} = 0.5$, $W_{fin} = 1\times10^{-2}$	Reference configuration

Due to the large number of test cases, a base case configuration is selected, defined by air as the working fluid ($Pr = 0.71$), a conductivity ratio of $k_{fin}/k = 1$, a fin length and vertical position of $L_{fin} = Y_{fin} = 0.5$, and a fin thickness of $W_{fin} = 1\times10^{-2}$. Each subsequent variation in the parametric study is performed by changing only one parameter at a time, while keeping all others fixed, to isolate its effect on heat transfer and flow dynamics.

This supplementary document provides additional data and visualizations that support the analysis presented in the main manuscript. It includes detailed tables of numerical results for varying fin parameters, as well as contour plots and Nusselt number profiles to illustrate the effects of Rayleigh and Prandtl numbers across different fin configurations.

List of Figures:

- Figure S1: Isotherms at different fin positions (Y_{fin}) for selected Ra and Pr.
- Figure S2: Streamlines at different fin positions (Y_{fin}) for selected Ra and Pr.

- Figure S3: Local Nusselt number along walls for various Y_{fin}, *Ra*, and *Pr*.
- Figure S4: Isotherms at different fin lengths (L_{fin}) for selected *Ra* and *Pr*.
- Figure S5: Streamlines at different fin lengths (L_{fin}) for selected *Ra* and *Pr*.
- Figure S6: Local Nusselt number along walls for various L_{fin}, *Ra*, and *Pr*.
- Figure S7: Isotherms at different fin thicknesses (W_{fin}) for selected *Ra* and *Pr*.
- Figure S8: Streamlines at different fin thicknesses (W_{fin}) for selected *Ra* and *Pr*.
- Figure S9: Local Nusselt number along walls for various W_{fin}, *Ra*, and *Pr*.
- Figure S10: Isotherms at different conductivity ratios (k_{fin}/k) for selected *Ra* and *Pr*.
- Figure S11: Streamlines at different conductivity ratios (k_{fin}/k) for selected *Ra* and *Pr*.
- Figure S12: Local Nusselt number along walls for various k_{fin}/k, *Ra*, and *Pr*.

List of Tables:

- Table S1: Investigated parameter ranges.
- Table S2: NNR vs. fin position (Y_{fin} = 0.3, 0.5, 0.7) for varying *Ra* and *Pr*.
- Table S3: NNR vs. fin length (L_{fin} = 0.3, 0.5, 0.7) for varying *Ra* and *Pr*.
- Table S4: NNR vs. fin thickness (W_{fin} = 0.001, 0.01, 0.1) for varying *Ra* and *Pr*.
- Table S5: NNR vs. thermal conductivity ratio (k_{fin}/k = 1, 10, 100) for varying *Ra* and *Pr*.
- Table S6: Optimal fin configurations and design guidelines by *Ra* and *Pr*.

S1. Effect of fin position for various Ra and Pr numbers

Figure S1. shows a detailed collection of isotherm plots depicting the thermal field changes in a square enclosure equipped with a horizontal adiabatic fin. The analysis is conducted across various Rayleigh and Prandtl numbers and three specific fin positions: Y_{fin} = 0.3, 0.5, and 0.7.

At the lowest Rayleigh number ($Ra \leq 10^2$), the thermal field is driven primarily by diffusion, regardless of the Prandtl number or the position of the fin, and showing nearly vertical isotherms that reflect minimal convective movement. The isotherms show negligible distortion or curvature around the fin, suggesting that buoyancy forces are too weak to induce significant fluid motion. The presence of the fin has little to no observable influence on the temperature distribution, and no thermal plumes or circulatory patterns are evident.

As *Ra* increases to 10^3 and 10^4, the isotherms exhibit noticeable curvature, indicating the gradual transition from conduction-dominated to convection-influenced heat transfer, with more pronounced curvature observed at $Ra = 10^4$ due to increased thermal convection. The influence of fin location becomes more evident in this regime as the fin alters plume structures. This transition is more pronounced at higher Prandtl numbers, particularly *Pr* = 10, where the isotherms curve more distinctly near the hot and cold walls, reflecting enhanced buoyant motion. When the fin is positioned lower (Y_{fin} = 0.3), the isotherms remain largely unchanged in the region under the fin due to limited flow development. In contrast, the isotherms are stretched near the top left and bottom

right corners because of the increased horizontal velocity, which helps dissipate heat faster. In the mid-fin scenario (Y_{fin} = 0.5), the fin induces a more symmetrical distortion of the isotherms. Therefore, the thermal field experiences the most significant disruption. Here, the fin intersects the central convective vortex, causing the warm plume to divide and reorganize, leading to tighter isotherm spacing and increased thermal gradients, especially in the region under the fin. At Y_{fin} = 0.7, the fin is placed in a region where the upward flow has become more established, primarily creating an obstructive effect. As a result, warm fluid is pushed laterally at the area beneath the fin, which thickens the thermal boundary layer and increases heat dissipation toward the center. On the other hand, the region above the fin experienced almost equally parallel isotherms, indicating that heat conduction is the dominant heat transfer mode in this region.

For $Ra = 10^5$, the thermal field becomes strongly convective, with compressed isotherms near the vertical boundaries and noticeable distortion around the fin. This behavior is more pronounced at a higher *Pr* number (*Pr* = 10.0). The presence and position of the fin strongly influence the thermal field. When placed at mid-height (Y_{fin} = 0.5), the fin causes a symmetrical deflection of isotherms above and below it, effectively splitting the convective cell. In contrast, at Y_{fin} = 0.3 or 0.7, the isotherms become more asymmetric, with more significant distortion on the side of the cavity containing a larger uninterrupted flow path. This behavior is particularly evident for *Pr* = 10.0, where thermal boundary layers are thinner and the effect of the fin is more pronounced. The flow exhibits complex thermal layering and stronger gradients, suggesting the emergence of recirculation zones even if they are not explicitly shown.

At $Ra = 10^6$, the isotherms display highly compressed and sharply contoured structures near the vertical walls, indicating the dominance of vigorous buoyancy-driven convection. The thermal boundary layers are extremely thin, particularly at higher Prandtl numbers, such as *Pr* = 10.0, where the temperature gradients are steep and closely packed near the hot and cold walls. The influence of fin position is substantial: when the fin is placed at mid-height (Y_{fin} = 0.5), it disrupts the symmetry of the thermal field by dividing the cavity into two distinct convective regions, with strong thermal stratification above and below. At Y_{fin} = 0.3, the isotherms bend sharply upward above the fin, suggesting intensified upward plume development. In contrast, at Y_{fin} = 0.7, the thermal field below the fin becomes compressed, and plume development is obstructed. The sensitivity to the Prandtl number is also evident, where low-*Pr* cases like *Pr* = 0.1 show a broader thermal boundary layer characterized by more diffuse isotherm spacing. In comparison, high-*Pr* fluids exhibit a thinner confined thermal boundary layer characterized by steeper isotherm gradients and better responsiveness to fin obstructions. Overall, the temperature field at this *Ra* reflects strong convection-dominated transport, heavily modulated by fin placement and fluid properties.

Figure S1 demonstrates how the fin's position significantly affects the thermal field's behavior in natural convection. At low *Ra*, conduction dominates, and the fin has minimal effect regardless of *Pr*. As *Ra* increases, placing the fin at mid-height (Y_{fin} = 0.5) enhances heat transfer by symmetrically disrupting flow and promoting mixing. A lower fin position (Y_{fin} = 0.3) aids plume development, while an upper placement (Y_{fin} = 0.7) obstructs upward flow, causing thermal stratification below. This effect is most pronounced for high-Pr fluids and becomes more critical in convection-dominated regimes. This thermal behavior can be further understood by examining the corresponding flow structures, which the streamline contours can reveal.

Figure S2 shows the streamline contours inside a square enclosure with a horizontal adiabatic fin, analyzed under laminar natural convection without considering turbulence. The study examines three fin positions (Y_{fin} = 0.3, 0.5, 0.7), six Rayleigh numbers from Ra = 10 to 10^6, and three Prandtl numbers (Pr = 0.1, 0.71, 10), while keeping all other parameters constant (L_{fin} = 0.5, W_{fin} = 0.01, k_{fin}/k = 1). These visualizations depict the gradual transition from conduction-dominant to convection-dominant conditions and emphasize the significant effects of fin position and fluid properties on the internal flow dynamics.

The streamlines at the low Rayleigh numbers ($Ra \leq 10^3$) are smooth and almost circular, showing a regime dominated by thermal conduction and minimal buoyancy effects. Furthermore, variations in Prandtl number have little influence on the streamline patterns. The fin introduces only a slight flow alteration depending on its vertical position. For Y_{fin} = 0.3, the fin shifts the primary vortex slightly upward, forming a weak secondary vortex beneath the fin. In contrast, the primary vortex is shifted slightly downward, with a weak secondary vortex appearing above the fin for Y_{fin} = 0.7. For Y_{fin} = 0.5, the fin symmetrically disrupts the buoyant path, dividing the primary vortex into two similar recirculation zones above and below the fin, which reflects a balanced thermal obstruction and a more evenly split convective structure.

At $Ra = 10^4$, natural convection becomes more prominent, intensifying the flow structures observed at lower Ra. For fin positions at Y_{fin} = 0.3 and 0.7, the streamline behavior remains similar to that observed at $Ra \leq 10^3$, but with stronger circulation and more pronounced secondary vortices due to enhanced buoyancy forces. The fin deflects the primary vortex either upward or downward while generating localized recirculation zones on the opposite side of the primary vortex. However, for Y_{fin} = 0.5, the previously observed symmetric flow pattern begins to break down, particularly at low Prandtl numbers. In this case, the higher thermal diffusivity leads to weaker thermal gradients and slower momentum development, causing the flow to favor one side of the cavity and resulting in asymmetrical vortex formation. This symmetry breaking reflects the increased sensitivity of the convective structure to thermal diffusivity when buoyancy forces are sufficiently strong to drive complex flow interactions but not yet dominant enough to enforce full symmetry around the fin.

At $Ra = 10^5$, the flow field exhibits strong convection with intensified and more complex vortex structures across all fin positions and Prandtl numbers. For Y_{fin} = 0.3, the primary vortex observed at lower Ra splits into two, with the lower vortex beneath the fin becoming more prominent and intensified. This is due to the fin's obstruction of the upward buoyant flow, which redirects the circulation and enhances secondary vortex formation in the lower region. At Y_{fin} = 0.5, the flow becomes noticeably asymmetric compared to lower Ra, especially sensitive to changes in Pr. For Pr = 10.0, a single tilted vortex appears, which is slightly deflected downward, reflecting stronger momentum but limited thermal diffusion. For Pr = 0.71, two vortices emerge, with the upper vortex shifting above the fin, indicating stratified circulation zones. In the low-Pr case (Pr = 0.1), the flow becomes highly fragmented, forming four vortices, with the upper vortex splitting into three smaller vortices. This complexity arises from the dominance of thermal diffusion over momentum, which disrupts coherent convection and promotes the development of multiple weaker cells. For Y_{fin} = 0.7, the flow generally mirrors the structure seen at $Ra = 10^4$, except for Pr = 0.1, where a third weak vortex appears near the top right corner. This additional vortex results from high thermal diffusivity and thin boundary layers, destabilizing the upper flow region and allowing localized recirculation.

At $Ra = 10^6$, the flow becomes highly dynamic and complex, characterized by vigorous convection, multiple vortices, and thin thermal boundary layers near the walls and around the fin. The streamlines reveal intensified circulation and rich vortex structures across all Prandtl numbers and fin positions. For $Y_{fin} = 0.3$, the primary vortex observed at lower *Ra* is split into four distinct vortices, and the vortex beneath the fin becomes significantly more intensified. This is due to the fin acting as a strong flow barrier, promoting enhanced plume deflection and shear layer instability below the fin as buoyant forces grow. At $Y_{fin} = 0.5$, the previously observed symmetric vortex structure is fully disrupted. For $Pr = 10.0$, a dominant vortex is tilted downward, while for $Pr = 0.71$, multiple asymmetric vortices emerge, with two shifting above the fin and two underneath the fin. In the low-*Pr* case ($Pr = 0.1$), the flow fragments into several weak vortices, with the upper region exhibiting dispersed, thermally driven circulation due to high thermal diffusivity and insufficient momentum to sustain coherent rotation. For $Y_{fin} = 0.7$, the flow structure remains asymmetric, with pronounced flow and additional recirculation zones scattered around the cavity, especially for $Pr = 0.1$. These behaviors are physically driven by the dominance of buoyancy forces at high *Ra*, which promotes plume instabilities, shear layer separation, and strong flow obstacle interactions. However, this behavior changes as the *Pr* number increases. For instance, the vortex above the fin is diminished for $Pr = 10.0$ as the fin obstructs the upward flow and restricts recirculation near the top. This suppression results from weak thermal diffusivity and strong upward buoyant forces being redirected around the fin, causing weakened vortex formation in the upper zone.

The findings indicate that the placement of the fin is crucial in determining the internal flow structure. Specifically, while a fin position of $Y_{fin} = 0.3$ supports plume formation with minimal disruption, a position of $Y_{fin} = 0.7$ causes blockage and stagnation at the top. In contrast, the mid-height configuration ($Y_{fin} = 0.5$) results in the most balanced and efficient convective flow pattern. Additionally, the Prandtl number influences the flow field by modifying the momentum and thermal diffusivity balance. Fluids with a high Prandtl number demonstrate more localized and sharper vortices and increased responsiveness to disturbances caused by the fin. These findings imply that positioning the fin at mid-height for laminar natural convection systems can significantly improve thermal efficiency by enhancing flow symmetry and mixing, especially for high-*Ra* numbers.

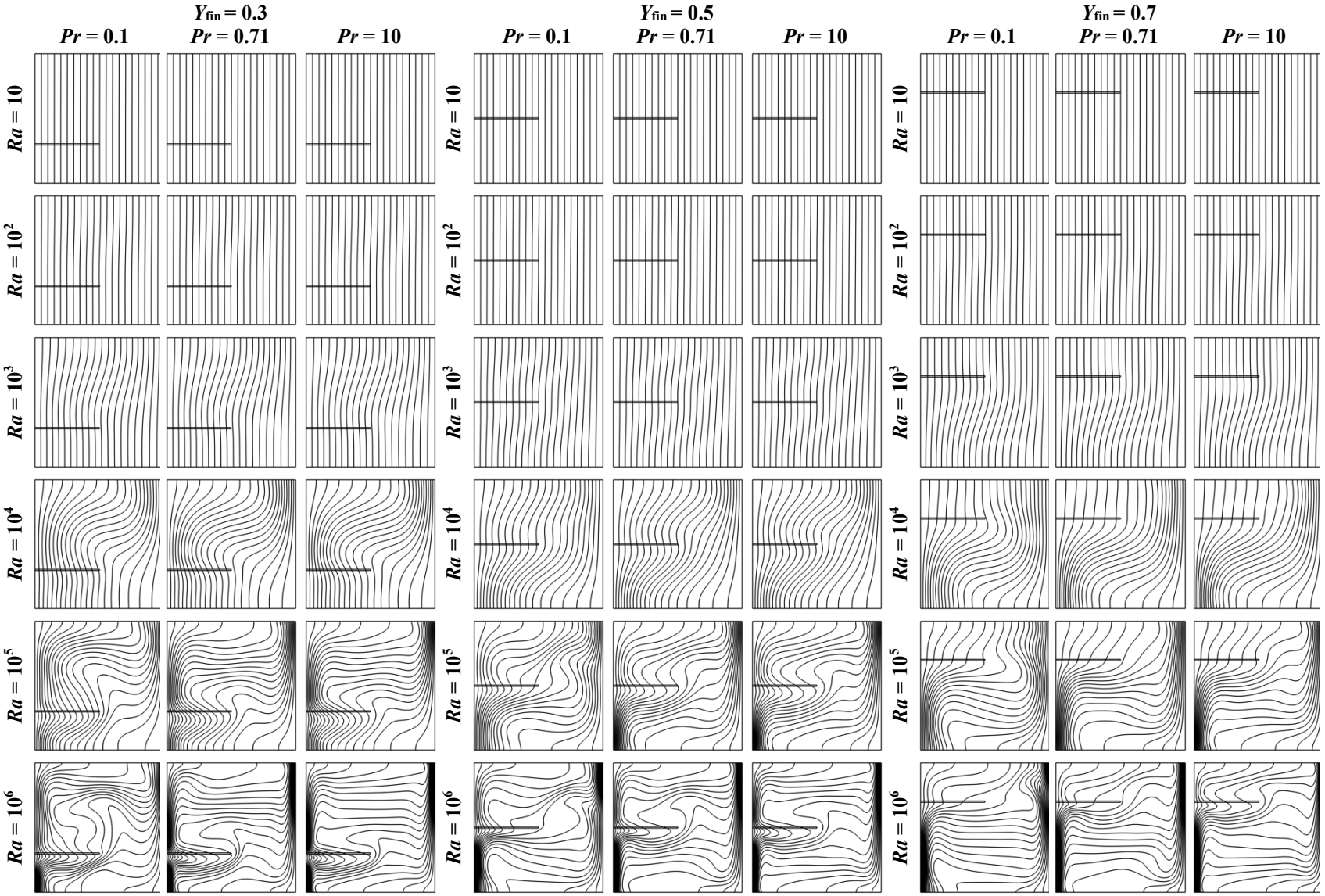


Figure S1. Isotherms of an enclosure with a fin for different *Ra* and *Pr* numbers at three fin positions (Y_{fin} = 0.3, 0.5, and 0.7), other parameters are fixed (L_{fin} = 0.5, W_{fin} = 0.01 and k_{fin}/k = 1).

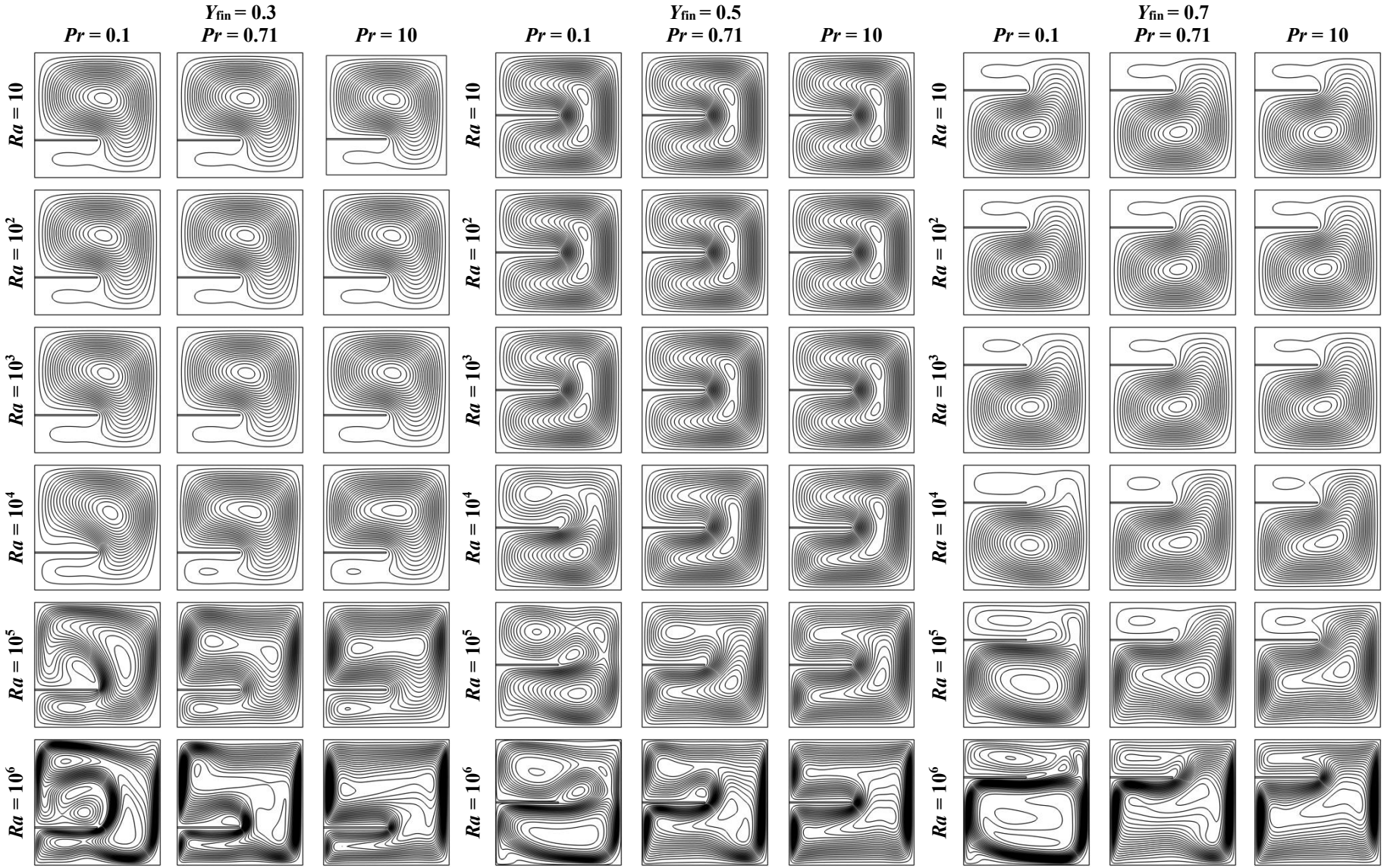


Figure S2. Streamlines of an enclosure with a fin for different *Ra* and *Pr* numbers at three fin positions (Y_{fin} = 0.3, 0.5, and 0.7), other parameters are fixed (L_{fin} = 0.5, W_{fin} = 0.01 and k_{fin}/k = 1).

Figure S3 shows the local Nusselt number (Nu_{loc}) variation along a square cavity's cold and hot vertical walls at three different horizontal fin vertical heights (Y_{fin} = 0.3, 0.5, and 0.7) for a wide range of Rayleigh numbers (Ra=10 to 10^6) and three Prandtl numbers (Pr=0.1, 0.71, and 10) under laminar natural convection conditions. The horizontal axis of Nu_{loc} along the cavity's cold wall is the dimensionless y-coordinate (Y) since there is no fin. In contrast, the hot wall has a fin. Therefore, the dimensionless distance (S) along the cavity's hot wall, beginning from the top-left corner and progressing downward, passing through the fin, is used as the horizontal axis of Nu_{loc} along the cavity's hot wall. Depending on the fin height, the fin's top face begins approximately at S = 0.7, 0.5, and 0.3 for Y_{fin} = 0.3, 0.5, and 0.7, respectively, and extends to the fin's right face, then the fin's bottom face, and finally, the rest of the wall.

In the pre-fin region (i.e., the upper section of the hot wall above the fin start), the thermal boundary layer develops due to buoyancy-driven flow. The local Nusselt number increases with higher Rayleigh numbers, consistent with enhanced convective heat transfer. Notably, for Pr = 10, the thermal boundary layer is thinner, resulting in sharper peaks of Nu_{loc} near the top edge. For instance, at Y_{fin} = 0.3, a sharp spike is seen near S ≈ 0.6, indicating intense thermal activity just after the fin obstructs the ascending thermal plume.

The introduction of the fin causes a noticeable disturbance in the thermal field. Over the fin surface, a pronounced modification in the heat transfer profile is observed since the fin interrupts the rising hot fluid, forcing it to either deflect laterally or circulate around the fin. This disruption leads to a sharp drop or localized peak in Nu_{loc}, depending on the flow strength and thermal gradients. At higher Ra, the ascending flow becomes stronger and more sensitive to obstructions, causing more distinct changes in local heat transfer. For high Pr, the sharper gradients result in elevated Nu_{loc} on the upper part of the fin, especially for Y_{fin} = 0.3, which is closer to the base and directly in the path of the main upward flow.

In the post-fin region, the boundary layer partially redevelops. As the warm fluid continues to rise and exits the fin region, there is typically a secondary growth in Nu_{loc}. This is especially prominent at high Ra, where inertia dominates, and the disrupted thermal plume reattaches or intensifies near the lower part of the wall. This plume is compressed toward the bottom corner for lower fin positions (e.g., Y_{fin} = 0.3), leading to a steep Nu_{loc} increase. In contrast, when the fin is placed higher (e.g., Y_{fin} = 0.7), the disturbance is closer to the top, and the lower region of the hot wall experiences more gradual boundary layer recovery.

Although the cold wall does not contain a fin, the presence of the fin on the hot wall significantly influences the temperature gradient and flow structure near the cold surface due to the induced clockwise natural convection in the cavity. Nu_{loc} generally increases with vertical position along the cold wall, and this trend becomes more pronounced at higher Ra. This is because buoyancy-induced convection enhances fluid motion and thinning of the thermal boundary layer, especially in the upper regions where the rising hot plume from the left wall impinges on the cold wall. Heat transfer is primarily conduction-dominated at low Ra = 10 or 10^2, resulting in relatively flat Nu_{loc} profiles. However, as Ra increases to 10^4 or higher, the influence of convection intensifies, causing a steep rise in Nu_{loc} along the wall, particularly in the upper half. For all fin positions, the highest Nu_{loc} values are consistently observed in the upper part of the cold wall (Y ≈ 1), where the thermal boundary layer is thinnest due to strong impinging flow. The profiles also reveal that the Prandtl number (Pr) plays a

crucial role in shaping the heat transfer behavior. Higher *Pr* values (e.g., *Pr* = 10) are associated with stronger temperature gradients and, consequently, higher Nu_{loc}. In comparison, lower *Pr* values (e.g., *Pr* = 0.1) correspond to more diffusive flows and gentler increases in Nu_{loc}.

Comparing the three cases, the fin position on the hot wall affects the cold wall indirectly. When the fin is located near the bottom (Y_{fin} = 0.3), it obstructs and diverts the initial upward flow, leading to stronger thermal mixing and plume formation that eventually reaches the upper cold wall with greater momentum. This results in a more pronounced rise in Nu_{loc}, especially in the *Ra* = 10^5 to 10^6 range. For the mid-wall fin position (Y_{fin} = 0.5), the convective influence becomes slightly more distributed, and the slope of Nu_{loc} along the cold wall remains steep but less abrupt than in the Y_{fin} = 0.3 case. When the fin is placed higher (Y_{fin} = 0.7), the upward thermal plume interacts with the cold wall earlier, but the disruption to the main ascending flow is weaker, resulting in smoother Nu_{loc} profiles.

In conclusion, the clockwise flow from left-wall heating causes hot fluid to rise along the finned surface. The presence and vertical position of the fin critically influence how this plume develops, deflects, and re-establishes downstream. Fins placed lower intercept the main rising thermal plume more effectively, leading to larger disruptions in Nu_{loc}, whereas higher fins primarily affect the upper recirculation structures. In contrast, although the cold wall is finless, the placement of a fin on the opposite hot wall alters the convection pattern. It significantly modulates heat transfer along the cold surface. The results emphasize the interconnected nature of enclosure convection, where modifications to one boundary (e.g., fin geometry on the hot side) propagate throughout the domain and reshape the thermal response on the opposing wall.

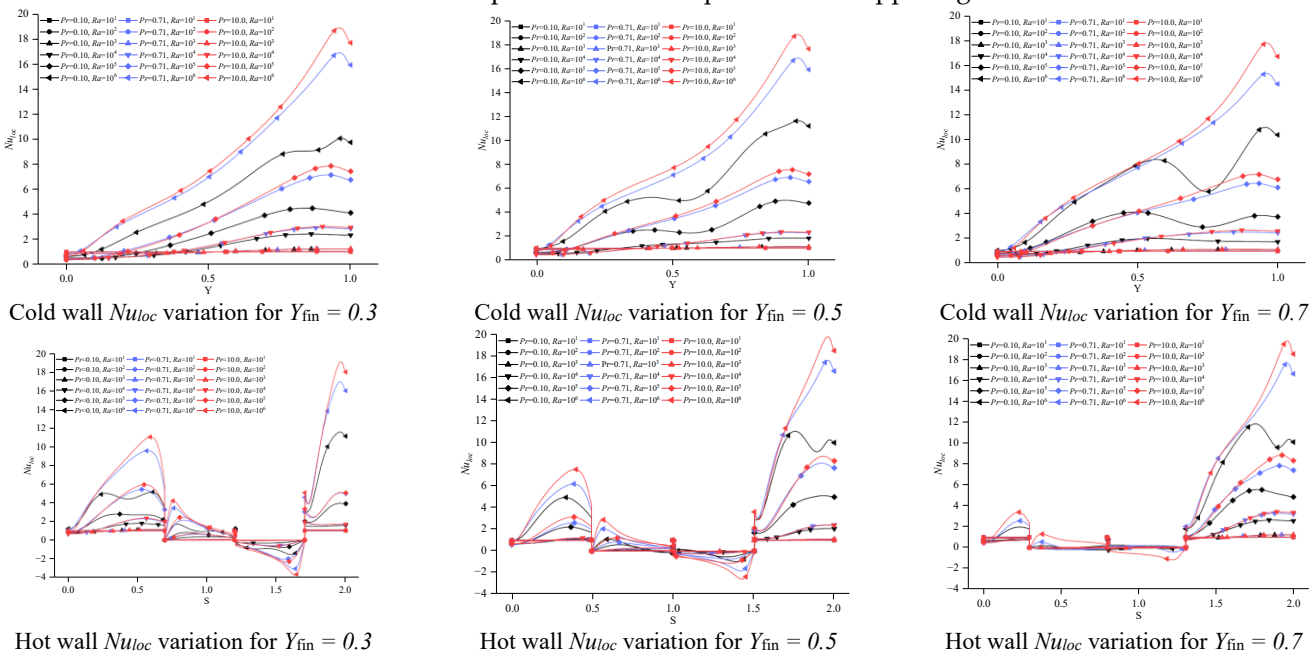


Figure S3. Variation of the Local Nusselt Number Along the Cold and Hot Walls of the Cavity for Different Fin Positions (Y_{fin} = 0.3, 0.5, and 0.7) at Various Rayleigh and Prandtl Numbers.

Table S2 illustrates the Normalized Nusselt Ratio (NNR) based on the Rayleigh number (*Ra*), Prandtl number (*Pr*), and fin position (Y_{fin} = 0.3, 0.5, and 0.7) within a square enclosure that contains a horizontal adiabatic fin. All other geometric and thermal parameters are held constant. The NNR is a dimensionless

indicator of how the fin's presence and placement enhance or hinder convective heat transfer. An NNR value of 1 signifies that the fin has no effect, whereas values below 1 indicate a reduction in heat transfer due to the fin's obstruction. This table demonstrates the shift in flow behavior from conduction-dominated to convection-dominated regimes as *Ra* increases. Furthermore, it illustrates how fluid properties, represented by *Pr*, interact with the fin's position.

At $Ra = 10$, characterized by a regime dominated solely by conduction, NNR values closely approximate unity across all *Pr* and Y_{fin} values, which range from 0.999986 to 0.999988. This near-optimal value indicates that the internal flow is negligible with minimal buoyant forces, and the fin has little to no effect on thermal performance. The thermal gradients are not strong enough to trigger convective recirculation, causing the enclosure's behavior to remain unchanged by the fin, irrespective of its position. This regime's maximum NNR over *Pr* (bold) values and maximum NNR over Y_{fin} (underline) values reinforce that all fin positions and Prandtl numbers are thermally equivalent, consistent with a purely diffusive regime.

At $Ra = 10^2$, the flow starts exhibiting slight buoyancy-driven behavior. However, the NNR values stay close to unity (≈0.9986–0.9988), indicating that conduction remains the primary mode of transport. The small differences in NNR across various Y_{fin} values and Prandtl numbers imply that fluid stratification and fin blockage are not significant enough to affect the overall heat transfer rate notably. Again, maximum NNR over *Pr* (bold) values cluster around the same *Pr*, and underlined values indicate that the top fin ($Y_{fin} = 0.7$) marginally favors convective transport, though the differences remain negligible.

As *Ra* reaches 10^3, the effects of natural convection become notably stronger. Consequently, the NNR values decline to the 0.90–0.92 range, indicating the beginning of convection-dominant behavior. The significance of the fin position becomes apparent, with the central fin ($Y_{fin} = 0.5$) resulting in the lowest NNR across all Pr values, suggesting a significant obstruction to convective pathways. In contrast, placing the fin closer to the bottom ($Y_{fin} = 0.3$) or top ($Y_{fin} = 0.7$) results in less disturbance of dominant flow structures, leading to slightly higher NNRs. The Prandtl number shows minimal influence in this range, although $Pr = 10.0$ yields slightly higher NNRs, likely due to more localized boundary layer development. This is reflected in the maximum NNR over Y_{fin} (underlined) values, which predominantly appear at $Y_{fin} = 0.7$, especially for high-*Pr* cases. The maximum NNR over *Pr* (bold) values for $Y_{fin} = 0.7$ corresponds to $Pr = 0.10$, highlighting its increasing thermal responsiveness.

For $Ra = 10^4$, the NNR values decrease further, especially for $Y_{fin} = 0.5$, which consistently exhibits the lowest ratio (≈0.59 to 0.60). The fin positioned at mid-height effectively disturbs the core thermal plume, splitting the cavity and hindering efficient convective circulation. Conversely, $Y_{fin} = 0.7$ yields the highest NNRs (≈0.73–0.78), indicating that placing the fin near the top helps maintain the upward flow, facilitating stronger heat transport. The effect of Pr becomes more evident, with elevated *Pr* values resulting in slightly increased NNRs, implying enhanced flow structuring and reduced damping from diffusion. Here, the maximum NNR over *Pr* (bold) value shifts to $Pr = 10$, and the maximum NNR over Y_{fin} (underlined) values consistently appear at $Y_{fin} = 0.7$, reinforcing the conclusion that the upper fin placement enables stronger convective performance in this regime.

At $Ra = 10^5$, a significant stratification is observed in the NNR responses. Notably, $Y_{fin} = 0.5$ no longer aligns with the minimum values; instead, it demonstrates a reversal, sometimes exceeding the performance of $Y_{fin} = 0.3$. This

change highlights a transformation in flow topology, where the central fin position promotes more symmetrical counter-rotating vortices, enhancing heat exchange on both sides of the fin. For Y_{fin} = 0.7, NNR values increase to 0.77–0.87, particularly at elevated Prandtl numbers. This supports the idea that fins positioned at the top allow vertical thermal plumes to ascend more freely, with limited flow separation appearing only in the upper regions. The significance of *Pr* becomes more pronounced, as *Pr* = 10.0 yields the highest NNRs, showcasing its ability to control flow and concentrate heat transfer. This trend is confirmed by the maximum NNR over *Pr* (bold) value in the *Pr* = 10 column and the maximum NNR over Y_{fin} (underlined) values appearing more frequently at Y_{fin} = 0.5 and 0.7 depending on the *Pr*.

At the highest Rayleigh number studied, $Ra = 10^6$, the enclosure functions in a regime dominated entirely by convection. In this scenario, the NNR values considerably broaden, starting from 0.72 for Y_{fin} = 0.3 and *Pr* = 0.1, and reaching as high as 0.94 for Y_{fin} = 0.5 and *Pr* = 10.0. The strong buoyancy forces lead to vigorous vortex formation, and their interaction with the fin generates highly localized thermal activity. In this regime, the influence of the Prandtl number becomes paramount. Fluids with high *Pr* (*Pr* = 10.0) maintain thinner thermal boundary layers that engage more effectively with the fin surfaces, promoting improved convective heat transfer, particularly when the fin is centrally placed (Y_{fin} = 0.5). Interestingly, the central fin position, which previously had the lowest NNR at moderate *Ra* (*Ra* = 1000), now exhibits the highest NNRs, reversing the earlier pattern. This indicates a dynamic shift in flow morphology caused by intensified mixing and symmetric vortex formation at mid-height, thereby optimizing heat transfer despite the geometric obstruction. The maximum NNR (bold and underlined) values at this *Ra* level reflects this reversal in performance, with the highest NNRs associated with Y_{fin} = 0.5 and *Pr* = 10.0.

In conclusion, the findings from **Table S2** illustrate a complicated interaction between fin placement, buoyancy intensity, and fluid characteristics. At low Rayleigh numbers, the fin's impact is minimal; however, as *Ra* rises, the location of the fin and the Prandtl number significantly influence thermal performance. Initially, placing the fin at the center (Y_{fin} = 0.5) most effectively hinders heat transfer, but it ultimately proves to be the most efficient setup under high *Ra* and *Pr* ≥ 1 conditions due to the enhancement of symmetric vortices. Additionally, the Prandtl number affects the extent of heat transfer improvements since higher *Pr* values allow for sharper thermal gradients and better use of convective channels. The bold and underlined values included in **Table S2** offer a concise visual summary of these effects, identifying optimal configurations for maximizing heat transfer in different thermal regimes.

Table S2. NNR of an enclosure with a fin for different *Ra* and *Pr* numbers at three fin positions (Y_{fin} = 0.3, 0.5, and 0.7). Other parameters are fixed (L_{fin} = 0.5, W_{fin} = 0.01 and k_{fin}/k = 1). Bold values indicate the maximum NNR across *Pr* for a given *Ra*. Underlined values indicate the maximum NNR across Y_{fin} for a fixed (*Ra*, *Pr*) combination.

Ra	Y_{fin}	***Pr* = 0.10**	***Pr* = 0.50**	***Pr* = 0.71**	***Pr* = 1.00**	***Pr* = 5.00**	***Pr* = 10.0**
10	0.3	0.999988	0.999988	0.999988	0.999988	0.999988	0.999988
	0.5	0.999986	0.999986	0.999986	0.999986	0.999986	0.999986
	0.7	0.999988	0.999988	0.999988	0.999988	0.999988	0.999988
100	0.3	0.998796	0.998796	0.998796	0.998796	0.998797	0.998797
	0.5	0.998604	0.998604	0.998604	0.998604	0.998604	0.998604
	0.7	**0.998799**	0.998798	0.998798	0.998798	0.998798	0.998798
1000	0.3	**0.915633**	0.915384	0.915405	0.915427	0.915491	0.915501
	0.5	**0.901113**	0.899746	0.899711	0.899697	0.899696	0.899698

	0.7	**0.918049**	0.916759	0.916691	0.916651	0.916591	0.916586
10000	0.3	0.670141	0.718964	**0.719662**	0.719390	0.718566	0.718600
	0.5	0.590534	**0.606303**	0.603928	0.601753	0.598077	0.597843
	0.7	0.730670	0.777240	0.779127	**0.779167**	0.776792	0.776403
100000	0.3	0.629054	0.796488	**0.798814**	0.798060	0.794815	0.794699
	0.5	0.681382	0.789783	0.803259	0.810365	0.818652	**0.819449**
	0.7	0.770055	0.851954	0.861231	0.866636	**0.870531**	0.869995
1000000	0.3	0.726227	0.880263	0.894521	0.902810	0.913963	**0.914935**
	0.5	0.815091	0.887793	0.901200	0.913453	0.937712	**0.939554**
	0.7	0.851272	0.897155	0.901969	0.906372	0.920580	**0.921424**

S2. Effect of fin length for various *Ra* and *Pr* numbers

Figure S4 displays the isotherm patterns within a square cavity containing a vertical fin at Y_{fin} = 0.5. Three fin lengths are examined in this figure, corresponding to L_{fin} = 0.3, 0.5, and 0.7. These visualizations cover a wide range of Rayleigh numbers from 10 to 10^6 and Prandtl numbers of 0.1, 0.71, and 10. The cavity functions in a conduction-dominated regime (without turbulence), maintaining a fixed fin width (W_{fin} = 0.01) and thermal conductivity ratio (k_{fin}/k = 1). At low Rayleigh numbers like Ra = 10 and 10^2, the isotherms stay mostly vertical, irrespective of fin length or Prandtl number. This setup indicates a heat transfer regime primarily controlled by conduction, where buoyancy effects are minimal, and the fin's geometric presence does not significantly alter the overall temperature distribution.

As Rayleigh numbers reach 10^3 and 10^4, the effects of natural convection become more evident, particularly for Pr = 0.71 and 10, where momentum diffusion is limited compared to thermal diffusion. The fin increasingly impacts the thermal field, especially with greater lengths. When L_{fin} is 0.7, the isotherms begin to curve more tightly around the fin, highlighting its increased thermal resistance and flow redirection. This curvature of the isotherms signifies the emergence of convective activity, where thermal energy follows intricate paths due to buoyancy-driven motion, and the fin serves as both a thermal and physical barrier within the cavity.

The Prandtl number plays a crucial role in the distribution of thermal energy. At Pr = 0.1, the high thermal diffusivity enables heat to spread rapidly within the enclosure, creating smoother isotherm lines even at elevated Rayleigh numbers. In contrast, at Pr = 10, the lower thermal diffusivity results in sharper temperature gradients, causing pronounced curvature of isotherms near the hot and cold walls as well as within boundary layers. The variation in isotherm density indicates the relative resistance to heat diffusion, with fluids of higher Pr displaying more concentrated thermal layers that highlight convective transport.

When Ra reaches 10^5, the isotherm profiles display increased complexity, revealing secondary circulations and more vigorous convection cells, especially near the fin tips. For longer fins like L_{fin} = 0.7, the thermal field shows marked asymmetry, with isotherms demonstrating sharp curvatures close to the fin-body junction, indicative of localized thermal disruptions and heightened natural convection. Such patterns suggest a stronger interaction between the fin and the fluid around it, resulting in increased thermal interference.

At a Rayleigh number of 10^6, convection becomes the primary mode of heat transfer, particularly when the Prandtl number is 0.71 or 10. The isotherms display layered, wave-like patterns that signify strong internal circulation. In these cases, longer fins enhance thermal interaction, with an L_{fin} of 0.7 causing the

most pronounced distortion and reorientation of the isotherms. Conversely, at a Prandtl number of 0.1, the solution does not converge at this high Rayleigh number. This issue likely results from numerical instability originating from high thermal diffusivity paired with fast buoyancy-driven flow. The thin thermal boundary layers and steep gradients complicate the conduction-based solver, particularly in the absence of turbulence modeling, leading to instability in the solution. In such conditions, thermal diffusion outweighs viscous effects, resulting in heightened sensitivity to numerical discretization and convergence parameters. Without very fine grids, higher-order methods, and strict solver tolerances, simulations may diverge or not converge due to significant local errors. This challenge is frequently noted in high-Rayleigh, low-Prandtl-number natural convection simulations, and it is well documented in research on thermal instability and the transition to turbulence in fluids such as liquid metals, which also exhibit low Prandtl numbers **[18, 19]**.

The length of the fin plays a crucial role in heat transfer patterns, particularly at elevated *Ra* and moderate to high Prandtl numbers. As the convective regime intensifies, isotherms transition from nearly vertical, conduction-driven lines to distorted patterns influenced by the fin's obstructive effect. The shift from diffusion-dominated to convection-dominated regimes is primarily dictated by *Ra* and *Pr*, with fin length serving as an essential modulator of the resulting thermal structure.

Figure S5 illustrates the streamlines of the development of natural convection within the enclosure based on *Ra*, *Pr,* and fin length L_{fin}, considering a single horizontal fin positioned at mid-height**.** At a low *Ra* of 10, regardless of the Prandtl numbers and fin lengths, the flow appears symmetric and weak, influenced mainly by conduction with minor disturbances around the fin. The circularity of the streamlines indicates limited convective motion, while longer fins (L_{fin} = 0.7) slightly disturb the central symmetry by redirecting flow around the fin tip, especially in fluids with higher Pr. As *Ra* rises to 10^2, the circulation becomes more vigorous, and convective cells show greater distinction. The effect of *Pr* becomes apparent—low *Pr* fluids (*Pr* = 0.1) maintain wider and more dispersed circulation zones due to greater thermal diffusivity. In contrast, high *Pr* fluids (*Pr* = 10) display tighter loops with sharper velocity gradients near the boundaries. The fin acts as a divider, separating the upper and lower circulations, particularly for L_{fin} measurements of 0.5 and 0.7, revealing clear stagnation zones at the fin tip.

At *Ra* = 10^3, the system experiences a shift towards convection-dominant behavior. With *Pr* = 0.1, the flow is smooth and characterized by large, weak eddies. In contrast, *Pr* = 0.71 and 10 exhibit significant recirculation cells above and below the fin. Here, the fin serves as a splitter, directing vertical flow into two main loops. For fin lengths of L_{fin} = 0.5 and 0.7, the flow strikes the fin's tip, resulting in separation and recirculation zones identifiable as dense streamline areas. As *Ra* increases to 10^4, buoyancy-driven flow intensifies. At *Pr* = 10, strong velocity jets form near the vertical walls while the central core exhibits vigorous rotation. Fins exceeding 0.3 in length start to markedly disrupt the symmetry of the streamlines, especially in the cases of *Pr* = 0.71 and 10, as the fin obstructs the ascent of hot plumes and splits the domain into two vortices, thus enhancing thermal mixing while causing local stagnation.

At *Ra* = 10^5, the flow evolves into intricate multicellular patterns. Streamlines maintain a more laminar and evenly spread configuration in low-*Pr* scenarios. In contrast, the flow develops into smaller eddies near the corners and around the fin tip in high-*Pr* situations. The primary cell migrates toward the

side opposite the fin base, suggesting a more pronounced plume deflection. Longer fins create sharper gradients, particularly evident in $L_{fin} = 0.7$, where the circulation zones asymmetrically expand around the obstruction. Lastly, at $Ra = 10^6$, the flow exhibits high dynamics and asymmetry, particularly for $Pr = 0.71$ and 10, as robust convective loops generate multiple recirculations in the lower and upper regions, while the central jet becomes more intense. The tips of the longer fins exhibit distinct stagnation zones, accompanied by secondary vortices. The $Pr = 10$ scenario presents the most intricate streamline evolution, as heightened viscosity limits diffusion and promotes vertical layering.

In every instance, a gradual increase in L_{fin} more aggressively divides the cavity, reducing direct vertical flow and boosting lateral recirculations. The Prandtl number influences thermal energy distribution, where low Pr scenarios are primarily diffusion-driven, while high Pr situations lead to increased concentration of energy and vorticity at the fin boundaries. The Ra number quantifies the intensity of buoyancy forces and directs the shift from conduction to convection-dominated processes. These results indicate that fin length significantly impacts flow structure, and its interaction with Ra and Pr regulates the formation of thermal stratification and vortex dynamics in natural convection.

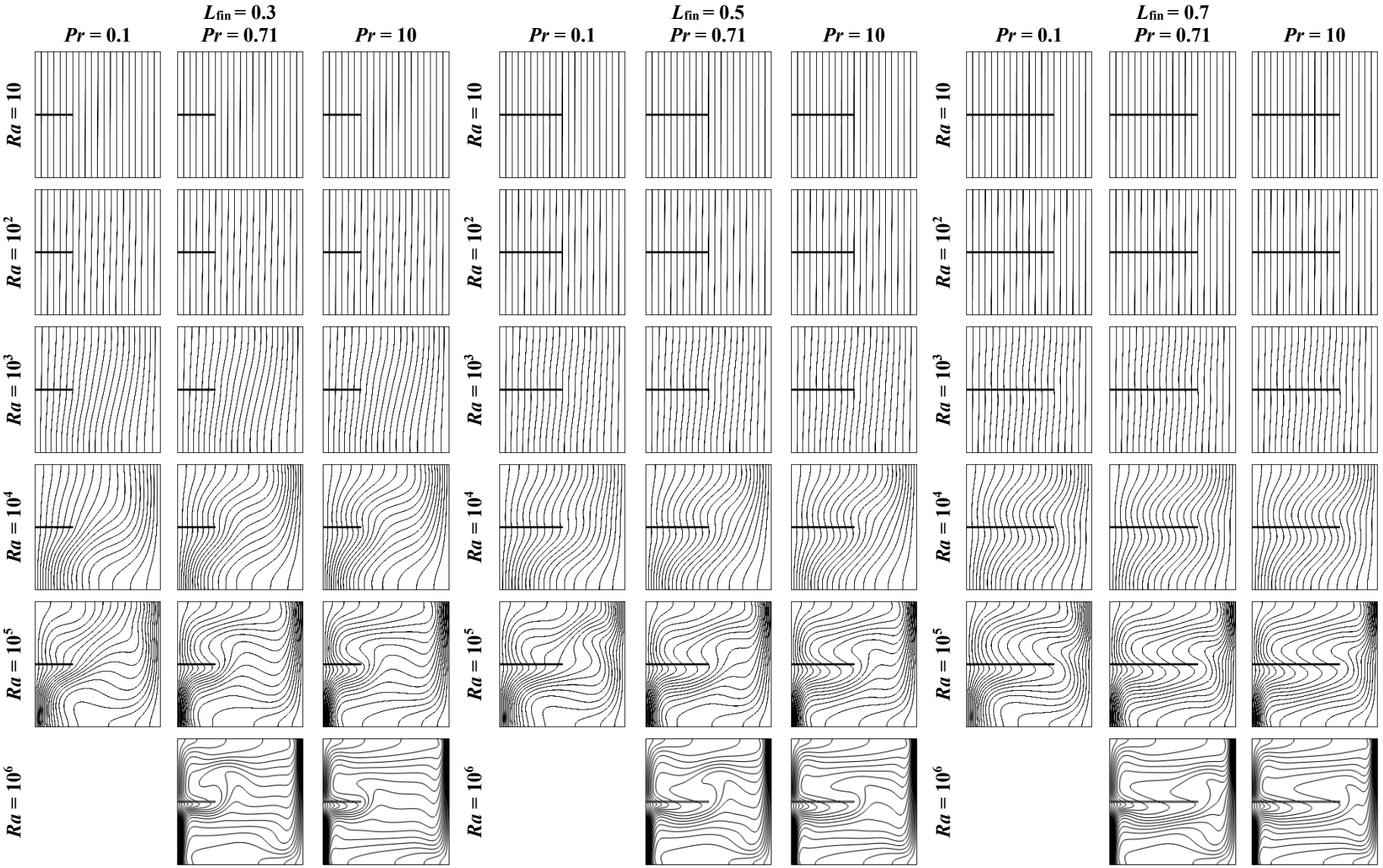


Figure S4. Isotherms of an enclosure with a fin for different *Ra* and *Pr* numbers at three fin lengths (L_{fin} = 0.3, 0.5, and 0.7), other parameters are fixed (Y_{fin} = 0.5, W_{fin} = 0.01 and k_{fin}/k = 1).

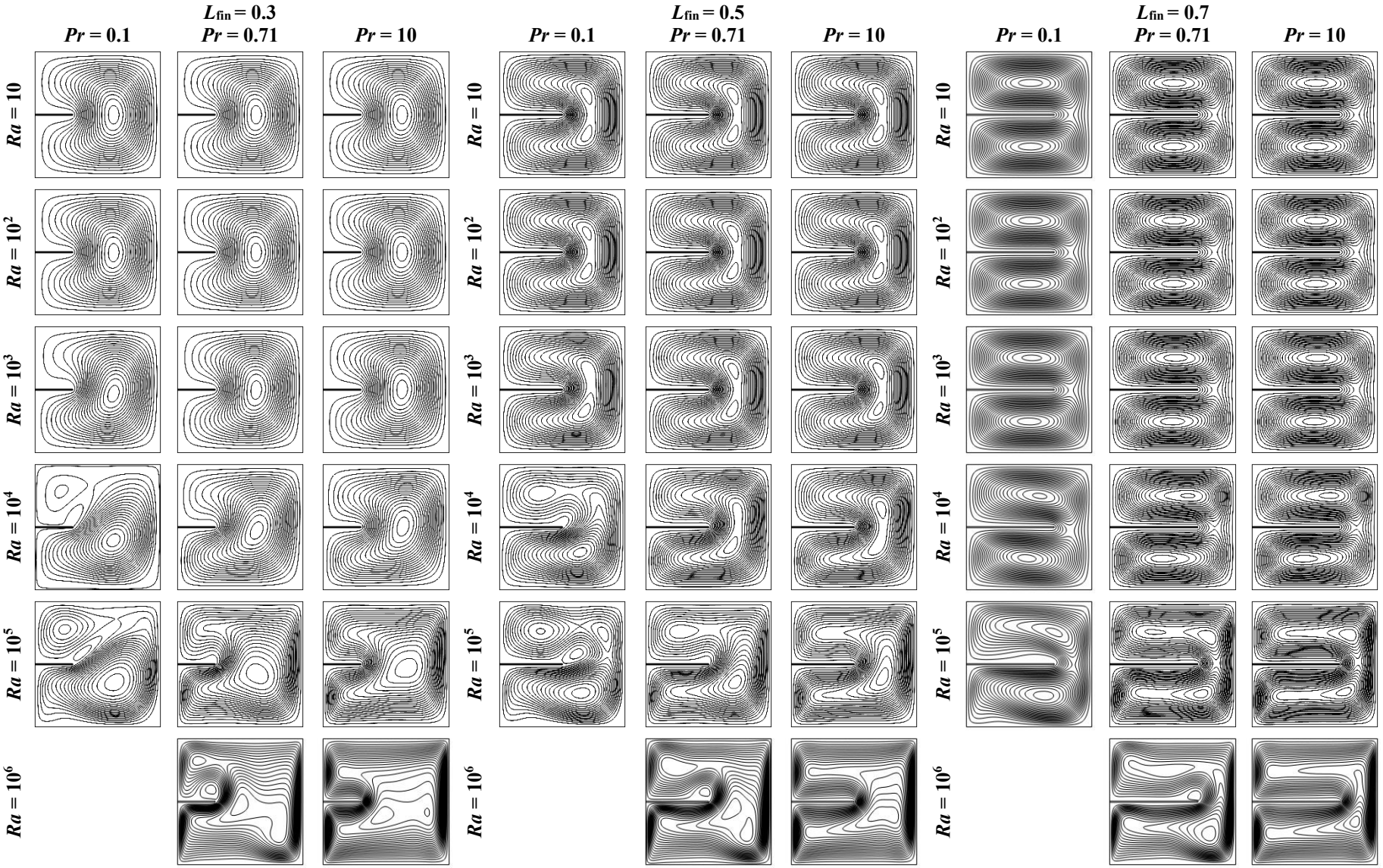


Figure S5. Streamlines of an enclosure with a fin for different *Ra* and *Pr* numbers at three fin lengths (L_{fin} = 0.3, 0.5, and 0.7), other parameters are fixed (Y_{fin} = 0.5, W_{fin} = 0.01 and k_{fin}/k = 1).

Figure S6 demonstrates the variations in the local Nusselt number (Nu_{loc}) along the cold and hot walls of the cavity, emphasizing how *Ra*, *Pr*, and L_{fin} influence local thermal gradients and flow structure in layers.

Starting from the cold wall, the general trend for all fin lengths indicates that Nu_{loc} increases with height (*Y*), with the steepest gradients observed near the top of the cavity. For low *Ra* values, such as 10 and 100, *Nu* varies gradually with elevation, suggesting that heat transfer is mainly dominated by conduction, especially for low-*Pr* fluids like *Pr* = 0.01. In these cases, the Nu_{loc} profiles are flatter and more uniform due to weak flow circulation and thicker thermal boundary layers, which limit vertical heat transfer improvements.

As the Rayleigh number rises to 10^4 and beyond, the effects of natural convection become increasingly significant. For *Pr* = 0.71 and 10, Nu_{loc} values increase sharply with *Y*, reaching peak levels near the top of the cold wall. This suggests a stronger buoyancy-driven flow close to the heated surface, where thermal boundary layers are thinned, particularly at higher *Ra* values. Fluids with higher Prandtl numbers, like *Pr* = 10, demonstrate overall greater Nu_{loc} values, indicating their lower thermal diffusivity and capacity to sustain steep temperature gradients near the wall.

Among the various fin lengths, the longest fin (L_{fin} = 0.7) exhibits the highest local Nu_{loc} near the cold wall's top for $Ra \geq 10^4$. This indicates that longer fins increase flow obstruction and promote boundary layer thinning by restricting convective cells, which results in stronger updrafts and a localized boost in convective transport. Conversely, for L_{fin} = 0.3 and 0.5, the enhancement in Nu_{loc} is observed but is comparatively moderate, as their impact on the convective structure and flow stratification is less significant.

Examining the hot wall reveals a more intricate Nu_{loc} distribution. The plots illustrate that at lower *Ra* and *Pr* = 0.01, the Nu_{loc} profiles remain mostly flat or only slightly inclined, indicating minimal convective activity and thick boundary layers dominated by conduction. As *Ra* increases, particularly at *Pr* = 0.71 and 10, distinct vertical gradients emerge near the upper wall, especially beyond the fin tip. These peaks align with localized areas where rising thermal plumes hit the hot wall or flow reattachment occurs. However, in contrast to the turbulent case, these peaks are wider and smoother, indicating a lack of intense mixing and the laminar flow's characteristics.

Specifically, longer fins lead to noticeable changes in the Nu_{loc} distribution. When L_{fin} = 0.7, a clear secondary peak forms downstream of the fin area, linked to laminar vortex creation that improves localized heat transfer. As L_{fin} reduces, the fin's effect on the overall Nu_{loc} profile diminishes, with wall heat transfer increasingly governed by conduction in the lower wall segments and weak convection near the top.

In summary, **Figure S6** depicts the fundamental characteristics of laminar natural convection in a finned cavity. The local Nusselt number distribution is affected by vertical position, thermal buoyancy (*Ra*), and fluid thermal diffusivity (*Pr*). The fin length is critical in modifying boundary layer development and enhancing Nu_{loc} near the fin tip. However, heat transfer profiles are comparatively uniform, predictable, and symmetrical. These findings underscore the need to consider transitional or turbulent effects at higher *Ra* to avoid underestimating peak heat transfer regions and to ensure accurate predictions of thermofluid behavior in practical engineering contexts.

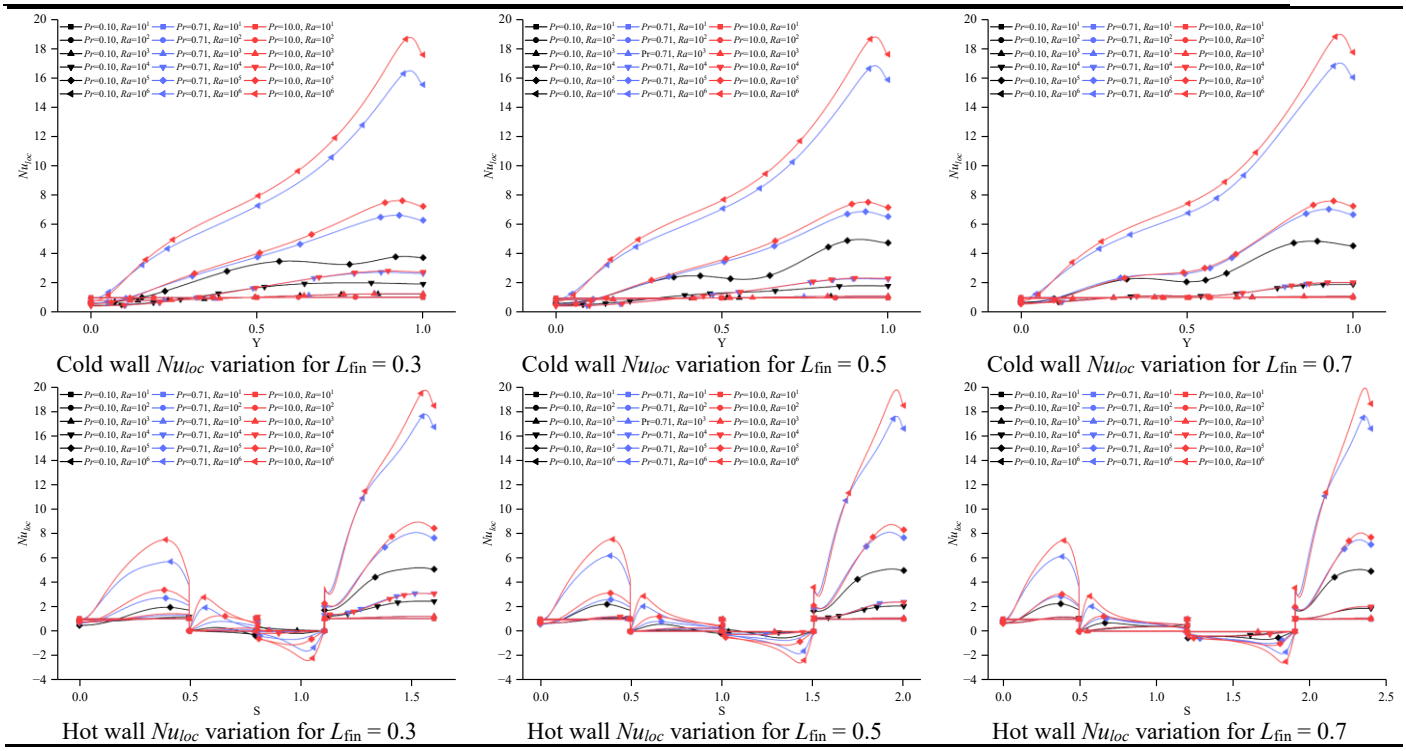


Figure S6. Variation of the Local Nusselt Number Along the Cold and Hot Walls of the Cavity for Different Fin Lengths (L_{fin} = 0.3, 0.5, and 0.7) at Various Rayleigh and Prandtl Numbers.

Table S3 illustrates how buoyancy (*Ra*), fluid thermal diffusivity (*Pr*), and geometric parameters (L_{fin}) collectively influence the NNR, a vital measure of a fin's ability to improve convective heat transfer compared to the baseline. NNR values near 1 indicate slight enhancement, while lower values suggest increased convective effects and a shift away from purely conductive behavior. Thus, this table outlines the shift from conduction-dominated to convection-dominated regimes.

At low Rayleigh numbers (*Ra* = 10 and 10^2), NNR values remain close to unity (≈ 0.999) across all Prandtl numbers and fin lengths. This indicates that conduction prevails, with buoyancy forces unable to initiate significant fluid movement. In this regime, the impact of fin length is minimal since heat transfer is mainly controlled by thermal diffusion within the stationary fluid. Additionally, changes in *Pr* have little effect because the flow field is suppressed. The maximum NNR (bold and underlined) values in this range are nearly indistinguishable, reaffirming that all fin lengths perform equivalently under conduction-dominated conditions.

As *Ra* reaches 10^3, NNR values begin to decrease slightly, signaling the start of buoyancy-driven movement. At this stage, the Prandtl number starts to have a more noticeable effect. For low-*Pr* fluids (*Pr* = 0.1), the NNR stays comparatively high (ranging from 0.9172 to 0.8990), indicating minimal convective influence due to the fluid's elevated thermal diffusivity. Conversely, for moderate to high-*Pr* fluids (*Pr* = 0.71 to 10), the NNR continues to decline slightly, particularly with longer fin lengths. This indicates that fluids with lower thermal diffusivity (i.e., higher *Pr*) facilitate more significant thermal gradients, thereby enhancing convective effects even in laminar flow conditions. The maximum NNR over *Pr* (bold) values at *Ra* = 10^3 occur at *Pr* = 0.1 across all lengths, while the maximum NNR over L_{fin} (underlined) values predominantly appear at L_{fin} = 0.3, highlighting that shorter fins maintain higher NNRs as convection emerges.

The effect becomes significantly more pronounced at $Ra = 10^4$. The NNR decreases markedly, reaching a low of 0.546 at $L_{fin} = 0.7$ and $Pr = 10$, showing that convection is now the primary mechanism for heat transfer. In this context, both fin length and Prandtl number play crucial roles. Longer fins (e.g., $L_{fin} = 0.7$) result in lower NNR values, particularly with higher-Pr fluids, due to greater flow obstruction and enhanced development of thermal boundary layers. The response across Pr is nonlinear; for example, at $L_{fin} = 0.3$, increasing Pr from 0.1 to 0.71 moderately boosts the NNR (from 0.668 to 0.732), but further raising Pr to 10 yields minimal or slightly reduced returns, indicating diminishing gains at elevated Pr due to saturation of convective efficacy. The maximum NNR over Pr (bold) values now appear at intermediate Pr values (e.g., $Pr = 1.0$) for $L_{fin} = 0.3$. In contrast, the maximum NNR over L_{fin} (underlined) values frequently occur at this shorter length across multiple Pr numbers, confirming its superiority under moderate convection conditions.

At $Ra = 10^5$, the pattern becomes clearer. For $Pr = 10$, NNRs peak at 0.868 when $L_{fin} = 0.3$ but decline with longer fins. This highlights a trade-off: while extended fins can enhance local temperature near the fin base, they hinder overall flow circulation and heat transfer efficiency. Specifically, with $L_{fin} = 0.7$, the NNR for $Pr = 10$ drops to 0.758, illustrating that excessively long fins may diminish thermal advantages in laminar flow. This is reflected in the maximum NNR over Pr (bold) values, which again align with $L_{fin} = 0.3$ at high Pr. The maximum NNR over L_{fin} (underlined) values for each (Ra, Pr) point to shorter or mid-length fins, rarely favoring $L_{fin} = 0.7$, even when Pr increases.

At $Ra = 10^6$, as natural convection nears turbulence, NNR values increase once more, particularly for fluids with high Prandtl numbers. For example, a Pr of 10 achieves a maximum NNR of 0.9497 at $L_{fin} = 0.3$. This increase indicates a shift in heat transfer efficiency, where convective mixing improves due to stronger buoyancy-driven flow. Notably, $Ra = 10^6$ data is absent for $Pr = 0.1$, possibly because of numerical constraints, but extrapolating from prior trends implies it would still be lower than that of high-Pr fluids. The maximum NNR over Pr (bold) values now reach their global peak at $L_{fin} = 0.3$ and $Pr = 10$, while maximum NNR over L_{fin} (underlined) values confirm this trend consistently across the row, marking the shorter fin as the optimal design for strong convection cases except for $Pr \leq 0.71$ where the peak occurs at $L_{fin} = 0.5$.

Table S3. NNR of an enclosure with a fin for different Ra and Pr numbers at three fin lengths ($L_{fin} = 0.3$, 0.5, and 0.7). Other parameters are fixed ($Y_{fin} = 0.5$, $W_{fin} = 0.01$ and $k_{fin}/k = 1$). Bold values indicate the maximum NNR across Pr for a given Ra. Underlined values indicate the maximum NNR across L_{fin} for a fixed (Ra, Pr) combination.

Ra	L_{fin}	***Pr* = 0.10**	***Pr* = 0.50**	***Pr* = 0.71**	***Pr* = 1.00**	***Pr* = 5.00**	***Pr* = 10.0**
10	0.3	0.999988	0.999988	0.999988	0.999988	0.999988	0.999988
	0.5	0.999986	0.999986	0.999986	0.999986	0.999986	0.999986
	0.7	0.999986	0.999986	0.999986	0.999986	0.999986	0.999986
100	0.3	0.998817	0.998817	0.998817	0.998817	0.998817	0.998817
	0.5	0.998604	0.998604	0.998604	0.998604	0.998604	0.998604
	0.7	**0.998580**	0.998579	0.998579	0.998579	0.998579	0.998579
1000	0.3	0.917226	0.917408	0.917414	0.917420	0.917439	**0.917442**
	0.5	0.901113	**0.899746**	0.899711	0.899697	0.899696	0.899698
	0.7	**0.899052**	0.897620	0.897584	0.897569	0.897567	0.897570
10000	0.3	0.668485	0.729678	0.732644	**0.733351**	0.732252	0.732018
	0.5	0.590534	**0.606303**	0.603928	0.601753	0.598077	0.597843
	0.7	**0.574298**	0.557151	0.553247	0.550456	0.546506	0.546310
100000	0.3	0.666313	0.808919	0.831802	0.846611	0.866981	**0.868409**

	0.5	0.681382	0.789783	0.803259	0.810365	0.818652	**0.819449**
	0.7	0.691751	0.773783	0.770659	0.766482	**0.758970**	0.758815
1000000	0.3	-	0.881434	0.900450	0.916959	0.947670	**0.949715**
	0.5	-	0.887793	0.901200	0.913453	0.937712	**0.939554**
	0.7	-	0.886218	0.896433	0.906231	0.928102	**0.929823**

In conclusion, the findings from **Table S3** demonstrate that fin length has a nonlinear impact on natural convection performance depending on the thermal regime. Short fins (L_{fin} = 0.3) are most beneficial in high-*Ra* and high-*Pr* conditions, enabling greater convective efficiency by minimizing flow obstruction. In contrast, longer fins (L_{fin} = 0.7) reduce overall NNR, especially at moderate to high *Pr*, by disrupting vertical plume development. The bold and underlined entries in **Table S3** indicate these trends, identifying L_{fin} = 0.3 as the dominant configuration in convection-dominated regimes and confirming that optimal fin length decreases as buoyancy intensifies.

S3. Effect of fin thickness for different *Ra* and *Pr* numbers

Figure S7 displays isotherm patterns that highlight how fin thickness (W_{fin}), Rayleigh number (*Ra*), and Prandtl number (*Pr*) significantly affect thermal distribution within the enclosure. An increase in *Ra* clearly displays a transition from conduction-dominated to convection-dominated regimes, prominently influenced by the fin geometry and fluid properties.

At low Rayleigh numbers (*Ra* = 10 and 10^2), the isotherms retain a nearly vertical and equidistant configuration, regardless of fin thickness or Prandtl number. This reflects a regime dominated by conduction with minimal convective influences. Such behavior is consistent with classical theory, which posits that buoyancy-driven flow is restricted due to weak thermal gradients and low thermal driving forces. In this range, fin thickness does not significantly change the isotherm shape, as the thermal boundary layer remains symmetric and undisturbed throughout the enclosure.

When *Ra* reaches 10^3, a slight curvature of isotherms appears near the fin area, particularly with thicker fins (W_{fin} = 0.1), indicating the onset of convection. At this stage, the Prandtl number influences thermal stratification; higher *Pr* (*Pr* = 10) results in more noticeable curvature and thicker thermal boundary layers adjacent to the vertical walls. This occurs because fluids with higher *Pr* exhibit lower thermal diffusivity, which enhances the effect of temperature gradients.

As *Ra* reaches 10^4, the thickness of the fin becomes crucial. With the thinnest fin (W_{fin} = 0.001), the isotherms near the fin remain relatively linear, suggesting that convective paths are only minimally obstructed. However, as W_{fin} increases to 0.01 and 0.1, a significant distortion of the isotherms around the fin is observed, indicating a greater disruption of heat flow pathways due to the larger cross-sectional area of the fin. This alteration increases local heat storage and changes the thermal transport dynamics. For *Pr* = 10, sharper gradients emerge near the fin-root junction, driven by a stronger link between the thermal field and diminished diffusion.

At *Ra* = 10^5, convective motion takes precedence, illustrated by the significant distortion and bending of isotherms, especially around the vertical walls and fin areas. For W_{fin} = 0.1, the temperature gradients are focused along the fin's sides, indicating that the thick fin acts as a thermal barrier, promoting stratification and enhancing recirculation zones. This effect intensifies at higher Prandtl numbers, with isotherms clustering more closely near the hot and cold walls, indicating steeper temperature gradients and more robust convective loops. The

temperature distribution becomes increasingly asymmetric, and the isotherms stretch vertically due to the heightened buoyant plumes.

At $Ra = 10^6$, the thermal field becomes very dynamic and complex. The narrowest fin (W_{fin} = 0.001) facilitates a more uniform temperature distribution, with the isotherms showing less distortion and smoother transitions between hot and cold sides. In contrast, with W_{fin} = 0.1, the isotherms become significantly nonlinear and compressed near the fin, revealing high local thermal gradients and complex convection rolls. The presence of high Prandtl fluids intensifies these gradients, highlighting the low thermal diffusivity and the strong influence of viscous forces compared to thermal diffusion.

Increased fin thickness significantly disrupts the thermal field, especially in convection-dominated situations. Thicker fins serve as barriers, altering the distribution of isotherms, amplifying temperature stratification, and diminishing thermal mixing within the enclosure. The Prandtl number additionally influences this phenomenon; greater *Pr* values enhance stratification and intensify thermal layering due to reduced thermal diffusion. The interaction between fin width (W_{fin}), Rayleigh number (*Ra*), and Prandtl number (*Pr*) shapes the overall heat transfer characteristics, where thinner fins behave in a thermally passive manner, while thicker fins substantially modify the convective structure.

Figure S8 provides a detailed illustration of the natural convection flow field within a square enclosure with a vertical fin at its center (Y_{fin} = 0.5). The fin maintains a constant height (L_{fin} = 0.5) and thermal conductivity ratio (k_{fin}/k = 1), while its thickness varies (W_{fin} = 0.001, 0.01, and 0.1). The streamlines present essential insights into the interaction between thermal and fluid properties, defined by Rayleigh and Prandtl numbers, and how these interact with geometric obstacles to influence flow behavior without a turbulence model. At the lowest Rayleigh number (Ra = 10), conduction prevails because of weak buoyancy forces, leading to predominantly stagnant fluid motion, with streamlines almost concentric and showing little circulation. This pattern persists across all Prandtl numbers and fin thicknesses, underscoring the prevalence of thermal diffusion over convective transport in low *Ra* scenarios.

As *Ra* reaches 10^2 and 10^3, buoyancy effects start to surpass viscous resistance, forming more organized flow cells. At this point, the influence of *Pr* becomes increasingly significant. For *Pr* = 0.1, which is typical for liquid metals, the flow is more dispersed due to high thermal diffusivity that quickly spreads thermal gradients and diminishes localized convection. The streamlines appear wider and flatter, suggesting that thermal conduction has a greater impact than momentum transfer. In contrast, for *Pr* = 10, representative of oils, low thermal diffusivity leads to closely spaced streamlines, reflecting vigorous flow near thermal boundaries. The slower heat diffusion than momentum allows temperature gradients to endure longer, enhancing buoyancy forces and forming distinct, symmetric vortex structures.

The impact of fin thickness becomes significantly pronounced when the Rayleigh number reaches 10^4, 10^5, and particularly 10^6, marking a shift from conduction-dominated to fully convection-driven transport due to natural convection. With a fin width of W_{fin} = 0.001, the fin is extremely thin. It causes minimal flow obstruction, enabling symmetric twin circulations to freely develop around it, primarily directed by buoyancy and the thermal boundary layers on the heated and cooled walls. However, as W_{fin} increases to 0.01, this obstruction starts to impact both the symmetry of the streamlines and the strength of the flow. The fin acts as a partial thermal and physical barrier, constraining vertical flow and causing recirculation zones to extend and shift laterally. This shift

becomes more noticeable at higher *Pr*, where viscous diffusion contributes to the stability of this flow deformation, resulting in vertically extended vortices that cling to the walls and flow separation near the fin tips.

When the fin reaches its maximum thickness (W_{fin} = 0.1), it significantly influences the flow pattern. In low-*Pr* conditions, the fin promotes thermal diffusion over its surface but restricts vertical fluid movement, leading to a decrease in convection strength in the center and an increase in lateral flow migration. For a *Pr* number of 10 at high *Ra*, the thicker fin obstructs rising thermal plumes, which causes the development of several secondary vortices and introduces asymmetry due to the competing influences of sidewall buoyancy and central fin resistance. The primary clockwise and counterclockwise cells, which initially rotated independently on each side, now interact through more intricate secondary circulations forming near the top and bottom of the fin. These phenomena are particularly pronounced at $Ra = 10^6$, where boundary layers become thinner and more susceptible to geometric changes. This regime's dense packing of streamlines signifies stronger convective currents and more delicate flow structures, showcasing the predominance of buoyancy-driven motion and the fin's capacity to either suppress or reroute thermal plumes based on its thickness.

This figure illustrates how a gradual increase in W_{fin} changes the enclosure from a nearly clear cavity to a heavily divided space. As a result, the flow dynamics shift from symmetrical buoyant recirculation to more asymmetrical and constrained flow patterns, with thermal gradients becoming more pronounced near the fins and walls. The interplay between fin design and the fluid's thermal properties affects not only the number and arrangement of vortices but also the thermal layering within the cavity. These findings are crucial for engineering applications like passive cooling in enclosures and heat sinks, where optimizing fin dimensions according to fluid type and thermal conditions is essential to enhance and control heat transfer. By omitting a turbulence model, the outcomes focus exclusively on laminar natural convection, making these insights particularly significant for systems experiencing moderate temperature gradients and limited geometries.

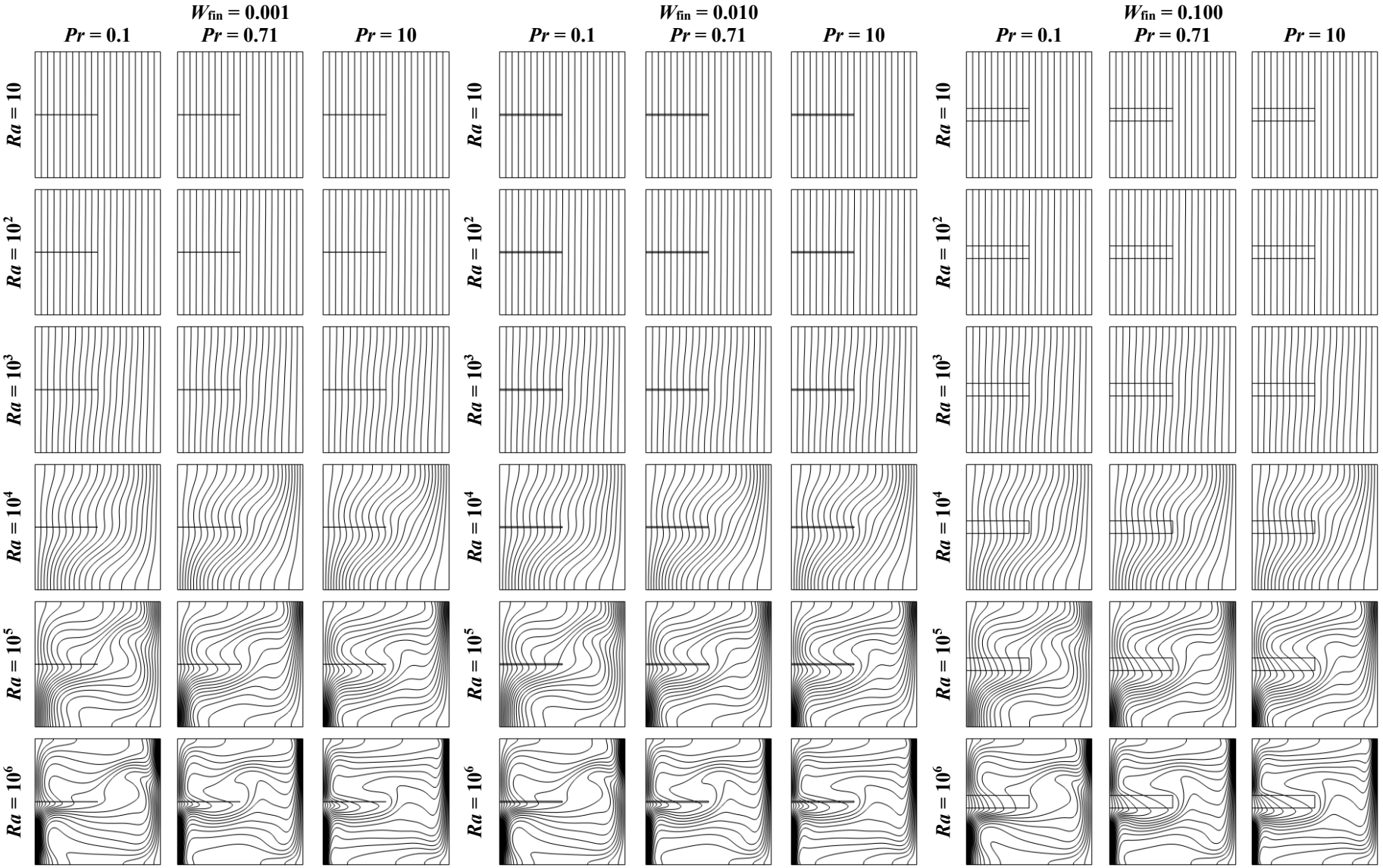


Figure S7. Isotherms of an enclosure with a fin for different *Ra* and *Pr* numbers at three fin thicknesses (W_{fin} = 0.001, 0.01, and 0.1), other parameters are fixed (Y_{fin} = 0.5, L_{fin} = 0.5 and k_{fin}/k = 1).

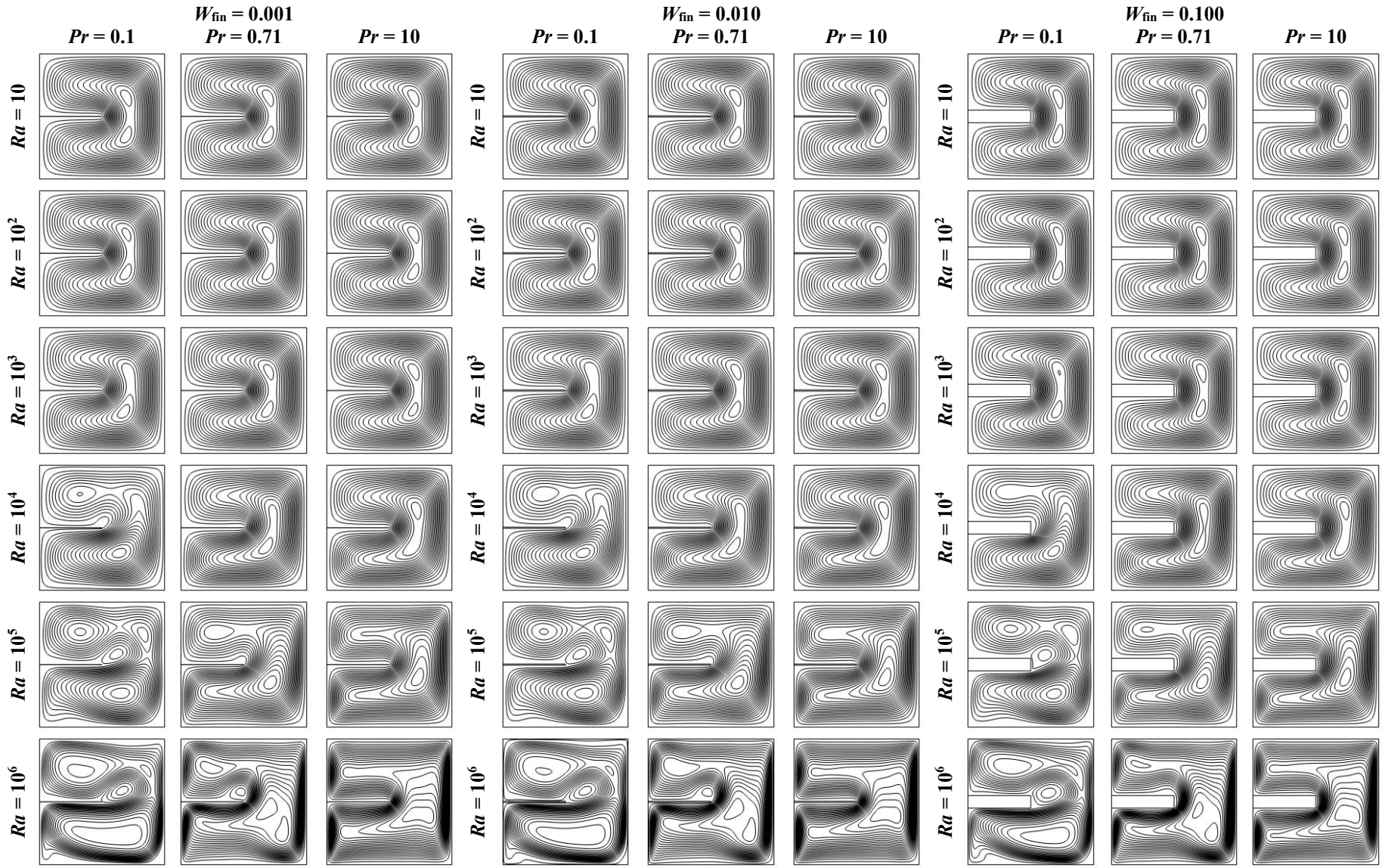


Figure 1. Streamlines of an enclosure with a fin for different *Ra* and *Pr* numbers at three fin thicknesses (W_{fin} = 0.001, 0.01, and 0.1), other parameters are fixed (Y_{fin} =

Figure S8. Streamlines of an enclosure with a fin for different *Ra* and *Pr* numbers at three fin thicknesses (W_{fin} = 0.001, 0.01, and 0.1), other parameters are fixed (Y_{fin} = 0.5, L_{fin} = 0.5 and k_{fin}/k = 1).

Figure S9 shows the distribution of local Nusselt numbers (*Nu*) along the cold and hot walls of the enclosure for three different fin thicknesses (W_{fin} = 0.001, 0.01, and 0.1), considering various Rayleigh (*Ra*) and Prandtl (*Pr*) numbers, all under laminar conditions without turbulence modeling. As the fin thickness increases from 0.001 to 0.1, the Nu_{loc} distribution on the cold wall is significantly impacted. With a W_{fin} of 0.001, the fin minimally disturbs the flow, which allows for unrestricted natural convection. This results in higher local Nu_{loc} values in the upper section of the wall, particularly at elevated *Ra* levels (like 10^5 and 10^6), indicating effective heat transfer. The increase in Nu_{loc} is especially notable for fluids with higher Prandtl numbers (*Pr* = 0.71 and 10.0), where the dominance of momentum diffusion enhances convective motion over thermal diffusion.

When the fin thickness rises to W_{fin} = 0.01, there is a noticeable drop in the local Nusselt number. The fin increasingly hinders the growth of the boundary layer, generating secondary vortices that modify heat transfer along the wall. This results in a minor decrease in the peak Nu_{loc} values, particularly at mid-height positions.

At W_{fin} = 0.1, the impact is markedly more disruptive. The thick fin introduces thermal and hydrodynamic blockage, obstructing vertical flow circulation and forming regions of thermal stagnation. Consequently, this results in a leveling off or slight reduction in local Nu_{loc} values, especially evident at low Prandtl numbers (e.g., *Pr* = 0.01), where thermal diffusion prevails over convective transport, leading to a decreased responsiveness of the system to localized flow accelerations.

Intriguing behavior unfolds on the hot wall. At W_{fin} = 0.001, distinct local peaks in *Nu* are observed near both the fin's base and tip, attributed to strong convective mixing from buoyancy-driven disturbances. When the thickness increases to 0.01, these peaks shift and decrease in intensity, as the thicker fin partially blocks thermal plumes. When W_{fin} = 0.1 is used, the Nu_{loc} profiles reveal broader areas of reduced heat transfer. This suggests that thicker fins impede hot fluid flow, particularly at higher *Ra* numbers where buoyant effects intensify.

Furthermore, the Prandtl number notably impacts the trends shown in **Figure S9** When *Pr* is high (*Pr* = 10.0), the thin thermal boundary layer reacts significantly to changes in geometry, causing a substantial suppression of Nu_{loc} with thicker fins. Conversely, thermal diffusion dominates at low *Pr* (*Pr* = 0.01), leading to more uniform Nu_{loc} distributions; nonetheless, thicker fins still produce lower values due to diminished flow interaction.

Figure S9 illustrates that thinner fins (W_{fin} = 0.001) enhance local natural convection heat transfer by promoting flow circulation and minimizing blockage. Conversely, thicker fins (W_{fin} = 0.1) act more as thermal resistances, impeding convective performance. This impact is especially pronounced at higher Rayleigh and Prandtl numbers, where the interaction between flow inertia and thermal gradients is more sensitive to fin geometry.

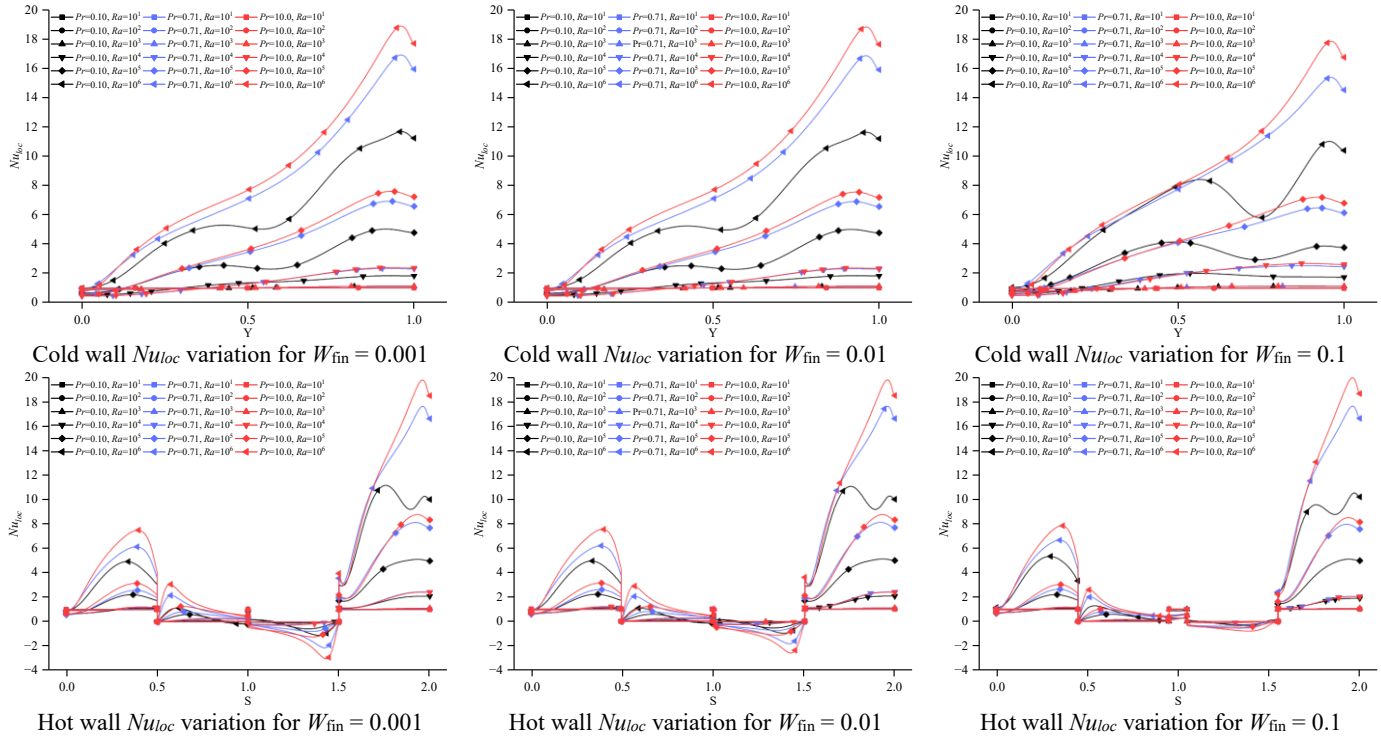


Figure S9. Variation of the Local Nusselt Number Along the Cold and Hot Walls of the Cavity for Different Fin Thickness (W_{fin} = 0.001, 0.010, and 0.100) at Various Rayleigh and Prandtl Numbers.

This examination of **Table S4** presents the Normalized Nusselt Ratio (NNR) for an enclosure equipped with a fin. The assessment is conducted at various Rayleigh (*Ra*) and Prandtl (*Pr*) numbers while utilizing three different fin thicknesses (W_{fin} = 0.001, 0.010, 0.100) under laminar flow conditions. All other parameters remain unchanged: fin vertical position Y_{fin} = 0.5, fin length L_{fin} = 0.5, and the thermal conductivity ratio k_{fin}/k = 1.

At very low Rayleigh numbers (*Ra* = 10), the Nusselt number ratio (NNR) stays nearly constant and close to one across different fin thicknesses and Prandtl numbers. This suggests that under conditions dominated by conduction, the thickness of the fins has minimal impact on the overall heat transfer rate within the cavity. Similarly, at $Ra = 10^2$, the NNR shows limited responsiveness to *Pr* and fin width. Although a slight decline in NNR occurs with increased fin thickness (from 0.998606 to 0.998581), this effect is negligible due to the low convective activity at this Rayleigh number. The maximum NNR over *Pr* (bold) values in this region appear indistinguishably close, reflecting uniformity in performance. The maximum NNR over W_{fin} (underlined) values also show no clear preference, indicating that all thicknesses behave similarly under conduction-dominated transport.

As *Ra* approaches 10^3, the influence of fin thickness becomes increasingly evident. For instance, at *Pr* = 0.10, the NNR decreases from 0.901318 at W_{fin} = 0.001 to 0.899219 at W_{fin} = 0.100. This pattern intensifies at *Ra* = 10,000, where NNR drops significantly as fin thickness increases. At *Pr* = 0.71, NNR falls from 0.608590 (W_{fin} = 0.001) to 0.555097 (W_{fin} = 0.100). This indicates that thicker fins more effectively impede convective flow, hindering thermal circulation and consequently lowering the effective Nusselt number compared to a cavity without fins. Notably, the Prandtl number exerts a moderate effect at this level, with higher *Pr* values typically resulting in slightly elevated NNRs, thanks to thinner thermal boundary layers that enhance heat transfer, even with resistance from

the fins. The maximum NNR over *Pr* (bold) values increasingly shift toward *Pr* = 10.0, and the maximum NNR over W_{fin} (underlined) values consistently appear at W_{fin} = 0.001, confirming the superior thermal performance of thinner fins in this transitional regime.

At $Ra = 10^5$, convective forces are the primary contributors to heat transfer, making the effect of fin thickness even more significant. For example, at *Pr* = 1.00, NNR decreases from 0.814129 at W_{fin} = 0.001 to 0.750593 at W_{fin} = 0.100. The reduction is even more pronounced at higher *Pr* values like 10.0. This suggests that increasing fin thickness diminishes the effectiveness of natural convection by limiting circulation zones and flow development, particularly close to the fin's base and tip, where recirculation and boundary layer separation are crucial. The maximum NNR over *Pr* (bold) values now clearly reside at *Pr* = 10.0 across all W_{fin}, while the maximum NNR over Wfin (underlined) values continue to favor W_{fin} = 0.001 for most *Ra*–*Pr* pairs, demonstrating that thin fins enhance buoyancy-driven circulation by minimizing flow resistance.

At the highest Rayleigh number tested ($Ra = 10^6$), the impact of fin thickness becomes more pronounced. The NNR at *Pr* = 0.71 decreases from 0.902616 for W_{fin} = 0.001 to 0.870758 for W_{fin} = 0.100. Yet, even with thicker fins, the NNR remains quite elevated at high *Pr* and *Ra*, indicating that robust buoyancy-driven flow at these conditions partly offsets the increased resistance due to thicker fins. Nonetheless, the steady decline of NNR with added fin thickness underscores the need for careful optimization of fin geometry, since thicker fins impede fluid movement and diminish convective heat transfer, even in strong natural convection scenarios. The maximum NNR over *Pr* (bold) values at $Ra = 10^6$ are highest at *Pr* = 10.0, and the maximum NNR over W_{fin} (underlined) values reinforce the consistent advantage of W_{fin} = 0.001 across nearly all high-*Pr* cases.

Table S4 illustrates that increasing fin thickness consistently leads to decreased NNR due to greater flow blockage and reduced convection, particularly at moderate to high *Ra*. This impact is limited in conduction-dominated situations (i.e. low-*Ra*) but becomes more significant as convection starts. Additionally, the effect of *Pr* becomes more noticeable at elevated *Ra* values, where fluids with higher Prandtl numbers maintain more substantial thermal gradients near boundaries, fostering improved local heat transfer even with thicker fins. These findings emphasize the necessity of optimizing fin thickness for effective thermal design in enclosures experiencing natural convection. The maximum NNR over *Pr* (bold) values emphasize the thermal advantage of high-*Pr* fluids, while the maximum NNR over W_{fin} (underlined) values confirm that thinner fins (W_{fin} = 0.001) are consistently superior under all convection-influenced regimes. These patterns together provide a valuable guideline for fin thickness optimization in natural convection systems.

Table S4. NNR of an enclosure with a fin for different *Ra* and *Pr* numbers at three fin thicknesses (W_{fin} = 0.001, 0.010, and 0.100). Other parameters are fixed (Y_{fin} = 0.5, L_{fin} = 0.5 and k_{fin}/k = 1). Bold values indicate the maximum NNR across *Pr* for a given *Ra*. Underlined values indicate the maximum NNR across W_{fin} for a fixed (*Ra*, *Pr*) combination.

Ra	W_{fin}	***Pr* = 0.10**	***Pr* = 0.50**	***Pr* = 0.71**	***Pr* = 1.00**	***Pr* = 5.00**	***Pr* = 10.0**
10	0.001	0.999986	0.999986	0.999986	0.999986	0.999986	0.999986
	0.010	0.999986	0.999986	0.999986	0.999986	0.999986	0.999986
	0.100	0.999986	0.999986	0.999986	0.999986	0.999986	0.999986
100	0.001	0.998606	0.998606	0.998606	0.998606	0.998606	0.998606
	0.010	0.998604	0.998604	0.998604	0.998604	0.998604	0.998604

	0.100	**0.998582**	0.998581	0.998581	0.998581	0.998581	0.998581
1000	0.001	**0.901318**	0.899964	0.899929	0.899915	0.899914	0.899916
	0.010	**0.901113**	0.899746	0.899711	0.899697	0.899696	0.899698
	0.100	**0.899219**	0.897803	0.897767	0.897752	0.897751	0.897753
10000	0.001	0.592908	**0.610655**	0.608590	0.606566	0.602997	0.602760
	0.010	0.590534	**0.606303**	0.603928	0.601753	0.598077	0.597843
	0.100	**0.561612**	0.558582	0.555097	0.552487	0.548634	0.548428
100000	0.001	0.685452	0.792055	0.806205	0.814129	0.823864	**0.824732**
	0.010	0.681382	0.789783	0.803259	0.810365	0.818652	**0.819449**
	0.100	0.636710	0.742273	0.748874	0.750593	0.751098	**0.751492**
1000000	0.001	0.819606	0.889347	0.902616	0.914965	0.940348	**0.942259**
	0.010	0.815091	0.887793	0.901200	0.913453	0.937712	**0.939554**
	0.100	0.761776	0.858703	0.870758	0.880473	0.899050	**0.900630**

S4. Effect of fin Conductivity ratio for different fin positions, *Ra* and *Pr* numbers

Figure S10 illustrates the isotherm distributions**,** offering a detailed perspective on the thermal activity in a square enclosure featuring a horizontal fin, influenced by natural convection across different Rayleigh numbers (*Ra*), Prandtl numbers (*Pr*), and thermal conductivity ratios of the fin (k_{fin}/k = 1, 10, 100). The simulations are based on a stationary fin positioned at mid-height (Y_{fin} = 0.5), with a length of L_{fin} = 0.5 and a thickness of W_{fin} = 0.01. Notably, all results are produced without turbulence models, thus emphasizing the effects of pure laminar natural convection.

With a low Rayleigh number of *Ra* = 10, the temperature distribution is almost linear throughout the enclosure, irrespective of the Prandtl number or the thermal conductivity of the fin. This reflects a conduction-dominated heat transfer. The isotherms are consistently spaced and vertically oriented, indicating negligible buoyancy forces, with heat primarily diffusing via thermal conduction. At this stage, the fin's influence is minimal, as the temperature gradient remains uniform and there is no significant convective motion to engage with the fin surface.

As *Ra* approaches 10^2, slight distortions start to emerge in the isotherms close to the fin and enclosure walls, particularly at elevated Prandtl numbers. These changes indicate the beginning of buoyancy-driven flow. The role of the Prandtl number becomes more apparent when examining fluids with higher *Pr* (i.e., *Pr* = 10), which display steeper gradients and more pronounced thermal boundary layers compared to those with lower *Pr* values. Nonetheless, the dominant mode of heat transfer remains conductive, especially in the low conductivity fin scenario (k_{fin}/k = 1), where thermal resistance restricts the heat distribution from the fin body.

At *Ra* = 10^3, convection becomes more significant, resulting in distinct isotherm curvature near the hot and cold walls. With lower Prandtl numbers like 0.1, the temperature field remains relatively diffuse, reflecting the high thermal diffusivity in low-*Pr* fluids, leading to weaker thermal gradients. On the other hand, fluids with higher Prandtl numbers (*Pr* = 0.71 and 10) exhibit more stratified isotherms and sharper thermal boundary layers near the fin and vertical walls. Increasing the thermal conductivity of the fin boosts its capability to conduct heat laterally. Furthermore, it distorts the nearby isotherms by more efficiently transporting heat from the hot side to the cold side. This effect is particularly evident at k_{fin}/k = 100, where the fin acts almost like an isothermal conductor.

Increasing *Ra* to 10^4 results in the formation of convective cells. The isotherms curve sharply around the fin tip, with steep gradients appearing near the hot wall and bending towards the cold wall. In scenarios with high *Pr,* the closer isotherm spacing at the boundary layers signifies greater thermal resistance and heightened temperature gradients. The effect of thermal conductivity becomes particularly evident in high-conductivity situations. When k_{fin}/k is 100, the fin enhances lateral heat transfer, altering the temperature distribution in the central region and creating more symmetrical isotherm patterns on both sides of the fin. Conversely, the fin with lower conductivity ($k_{fin}/k = 1$) struggles to transfer heat effectively, causing isotherms to cluster tightly on the hot side while flattening near the fin surface.

At $Ra = 10^5$, the system enters a strong natural convection regime. The temperature gradients near the hot wall and along the fin become more pronounced, showing signs of thermal plume formations. With $Pr = 0.1$, the thermal field stays spread out, while for $Pr = 0.71$ and 10, distinct isotherm clustering indicates the development of thermal boundary layers and recirculation zones. The high conductivity fin enhances this effect by conducting heat deep into the enclosure, effectively functioning as a secondary heat source and modifying the natural convective patterns around the fin.

At the highest Rayleigh number analyzed, $Ra = 10^6$, robust convection governs the thermal field. Isotherms arrange into distinct layers near the hot and cold walls, while the central region reveals plume-like structures and steep gradients. In this condition, the Prandtl number plays a crucial role: fluids with low *Pr,* such as $Pr = 0.1$, maintain relatively smooth gradients, whereas $Pr = 10$ results in sharp, closely packed isotherms. The fin's conductivity significantly alters these patterns. When $k_{fin}/k = 100$, the fin efficiently conducts heat, impacting the entire central domain and visibly distorting the isotherms, thereby modifying the core convective flow. Conversely, at $k_{fin}/k = 1$, the insulating properties of the fin confine the temperature field around it, having minimal effect on the central enclosure.

The streamline patterns shown in **Figure S11(a)** illustrate how varying Rayleigh (*Ra*) and Prandtl (*Pr*) numbers, along with thermal conductivity ratios (k_{fin}/k), influence natural convection flow within an enclosure featuring a single fin. These flow structures are produced without a turbulence model, enabling us to focus solely on the effects of buoyancy and thermal properties on the evolution of streamlines and vortex formation. At the lowest Rayleigh number ($Ra = 10$), conduction prevails, and buoyancy-driven convection is weak for all *Pr* and k_{fin}/k values. For $Pr = 0.1$, indicating high thermal diffusivity, the flow field is nearly symmetric and primarily driven by diffusion, displaying a single large vortex that fills the entire enclosure. The streamlines are smooth and widely spaced, suggesting slow, uniform circulation with little interference from the fin. As *Pr* rises to 0.71 and then to 10, momentum diffusion grows more significantly than thermal diffusion, leading to slightly tighter vortex structures and denser streamlines around the center and boundaries. Nevertheless, due to the very low *Ra*, these changes are subtle. The fin conductivity effect is restricted mainly to localized distortions of streamlines near the fin tip, without creating secondary flow zones.

As *Ra* approaches 10^2, buoyancy effects become increasingly noticeable, enhancing the flow. At this point, differences in the Prandtl numbers start to emerge more clearly. For $Pr = 0.1$, the flow continues to be diffusion-dominated, with a streamline pattern akin to that at $Ra = 10$, though the vortex tightens slightly. With *Pr* values of 0.71 and 10, the vortex becomes more concentrated

and rises due to stronger thermal gradients and buoyancy. This also leads to a rise in streamline density, particularly near the fin tip. The fin acts as a localized barrier, intensifying velocity gradients around it. However, the effect of increasing k_{fin}/k from 1 to 100 remains limited at this *Ra* level, as the thermal energy is still insufficient to produce vigorous convective motion. The streamline's structure retains a predominant single-cell pattern across all k_{fin}/k ratios.

When *Ra* reaches 10^3, natural convection becomes significantly more pronounced. At *Pr* = 0.1, the vortex strengthens while maintaining a relatively symmetric pattern, leading to a slight split in the vortex core due to the fin's influence. The high thermal diffusivity reduces temperature gradients, consequently limiting the enhancement in momentum transfer. At *Pr* = 0.71, the central vortex gains energy, exhibiting denser streamlines around the fin with noticeable inflections where the flow interacts with the solid structure. This behavior intensifies at *Pr* = 10, where thermal diffusion is diminished, facilitating the development of stronger gradients. Furthermore, the increased viscosity results in a more structured vortex with sharper circulation paths near the fin. An increase in k_{fin}/k from 1 to 100 slightly enhances the localized bending of streamlines, as the highly conductive fin acts as a thermal bridge, efficiently transferring heat from the hot left wall and modifying nearby flow paths. Nonetheless, the overall flow topology remains single-cell, with only minor internal distortions reflecting moderate thermal conductivity sensitivity.

As the Rayleigh number rises to 10^4, the flow shifts into a more convective regime. For *Pr* = 0.1, multiple vortex zones begin to develop as thermal and momentum diffusion mechanisms compete. The flow around the fin becomes increasingly asymmetric, with the lower cell shifting downwards, emphasizing the stronger effects of buoyancy and wall interaction. When *Pr* = 0.71, the primary vortex is pushed towards the top-right corner, and secondary recirculation starts to form beneath the fin. The fin disrupts the flow field significantly, especially at higher k_{fin}/k *values*, where heat conduction along the fin intensifies localized buoyancy forces. At *Pr* = 10, the flow changes dramatically, streamlines are more tightly clustered, and the vortex core becomes distinctly asymmetric. The interplay of low thermal diffusivity and high *Ra* leads to robust convection loops. As k_{fin}/k increases, the distortion of streamlines around the fin becomes more noticeable, particularly at k_{fin}/k = 100, where the conductive fin enhances thermal exchange with the surrounding fluid, intensifying circulation near its edges.

At *Ra* = 10^5, convection is entirely dominant. When *Pr* = 0.1, the flow features large, asymmetric vortices that are visibly distorted and partially split due to the fin's effect. Compared to lower *Ra* values, the flow field exhibits greater chaos, and a rise in k_{fin}/k seems to intensify this influence, with higher thermal conductivity pushing the streamline convergence zones toward the top-right corner. At *Pr* = 0.71, two distinct vortices develop: one above and one below the fin, indicating a strong interaction between the fluid and fin surfaces. The fin disrupts the primary convective loop, causing significant bending and tighter recirculation zones, especially as k_{fin}/k increases. With *Pr* = 10, convection cells take on a more structured and confined form, featuring clearly defined cores and minimal symmetry. The fin plays a crucial role in altering streamline topology, while an increase in thermal conductivity enhances this effect by boosting localized buoyancy-driven motion.

At *Ra* = 10^6, vigorous natural convection prevails for all *Pr* values. For *Pr* = 0.1, the flow becomes notably nonlinear, leading to large chaotic structures and numerous recirculation cells within the cavity. The fin divides the flow

vertically, creating separate recirculation regions above and below it. Enhanced thermal conductivity produces even more intricate patterns, as heat transfer along the fin promotes flow bifurcation. When $Pr = 0.71$, the flow exhibits well-defined vortices with significant velocity gradients, while the fin significantly influences the flow topology. Streamlines become tightly clustered, particularly near the hot wall and the fin's surface. At $Pr = 10$, the streamlines form a well-structured yet asymmetric vortex system, with vigorous boundary layer flows adhering closely to the walls. The fin acts as a dynamic modifier of the flow, with its thermal conductivity greatly influencing circulation zones, especially when $k_{fin}/k = 100$. At this stage, the interaction of high viscosity, low thermal diffusivity, and strong buoyancy results in very sensitive and uneven streamline distributions. The behavior of the enclosure is primarily driven by the combined effects of *Ra*, *Pr*, and fin conductivity, with each parameter increasingly complicating the flow structure.

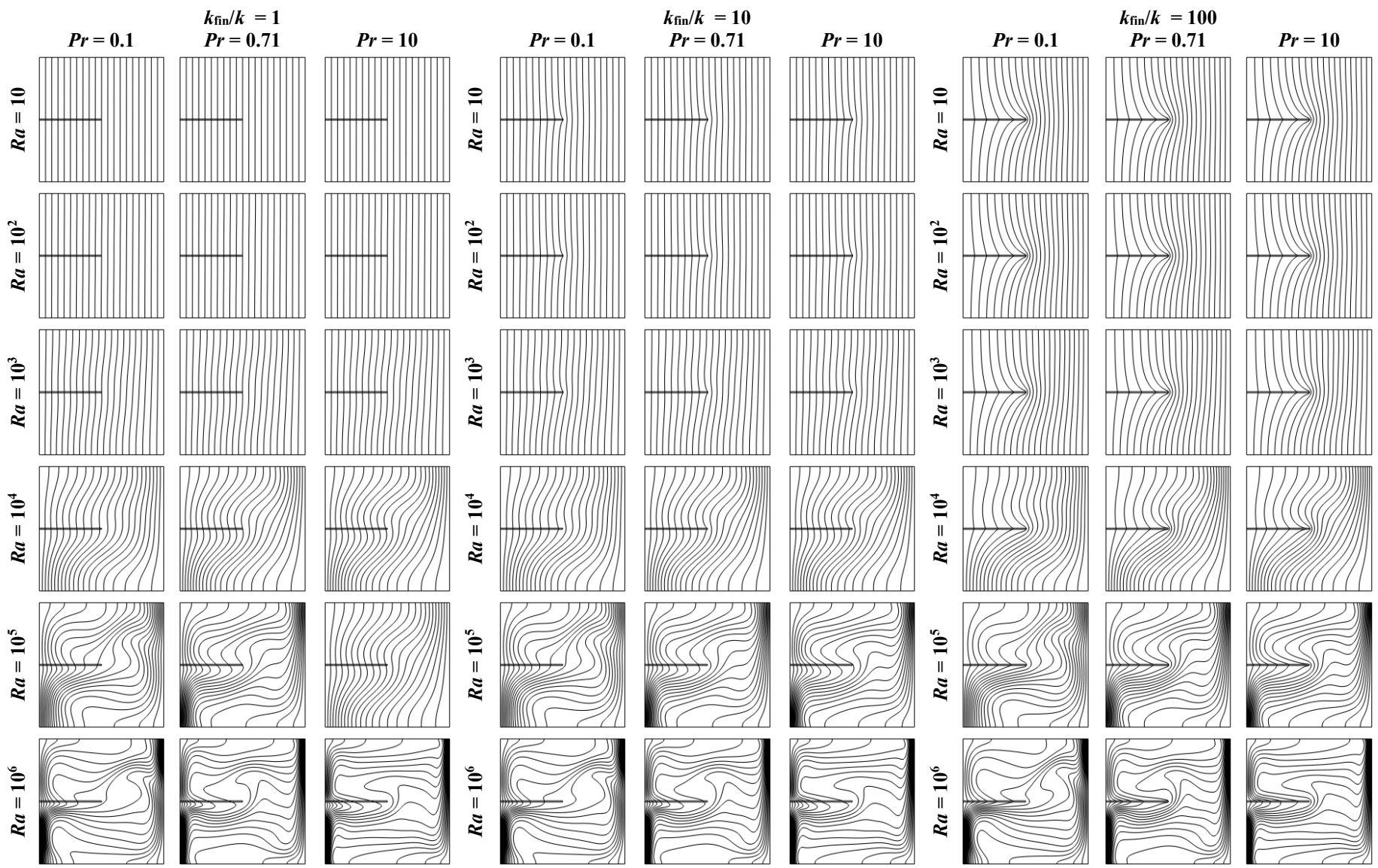


Figure S10. Isotherms of an enclosure with a fin for different *Ra* and *Pr* numbers at three thermal conductivity ratios (k_{fin}/k = 1, 10, and 100), other parameters are fixed (Y_{fin} = 0.5, L_{fin} = 0.5 and W_{fin} = 0.01).

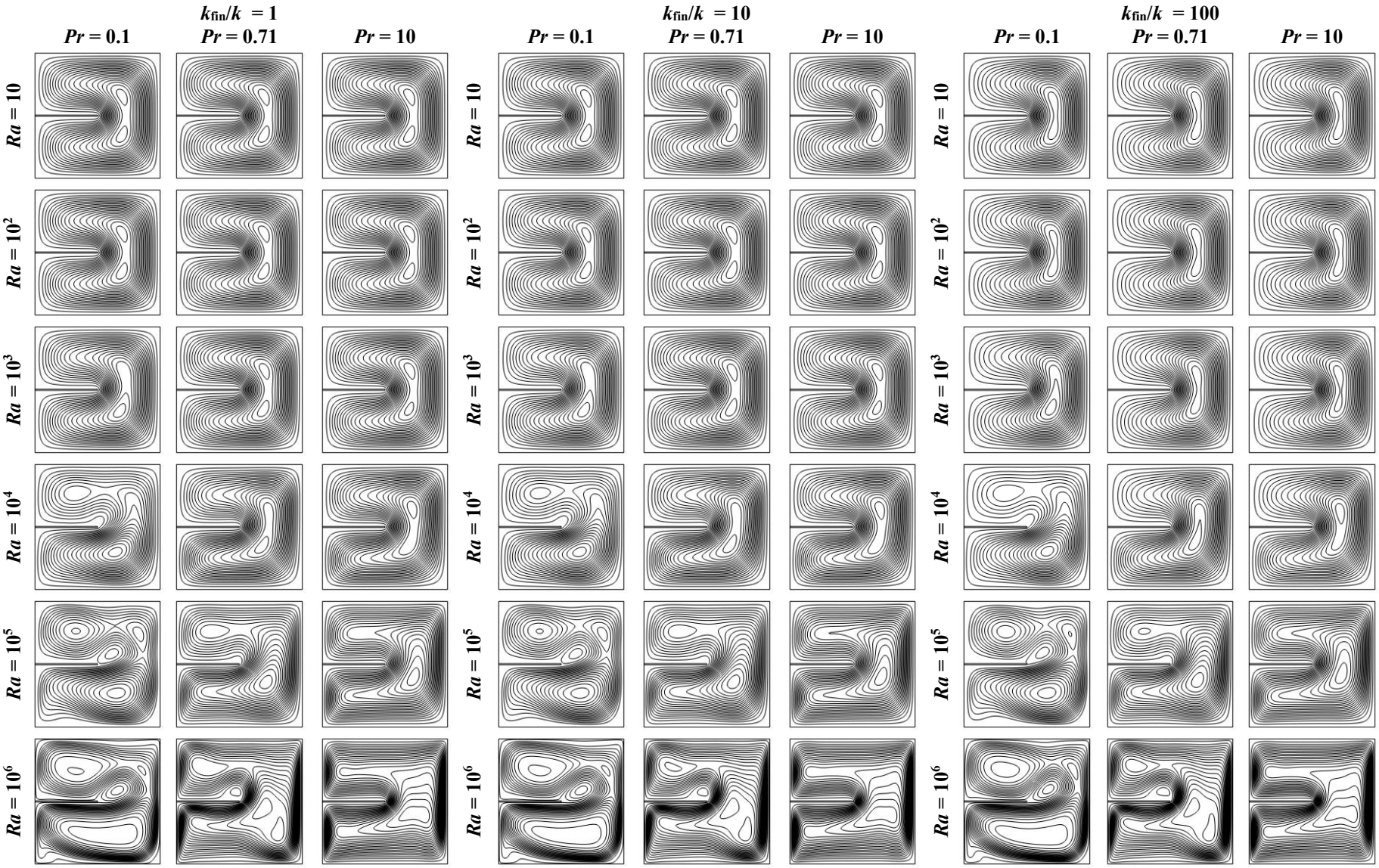


Figure S11. Streamlines of an enclosure with a fin for different *Ra* and *Pr* numbers at three thermal conductivity ratios (k_{fin}/k = 1, 10, and 100), other parameters are fixed (Y_{fin} = 0.5, L_{fin} = 0.5 and W_{fin} = 0.01).

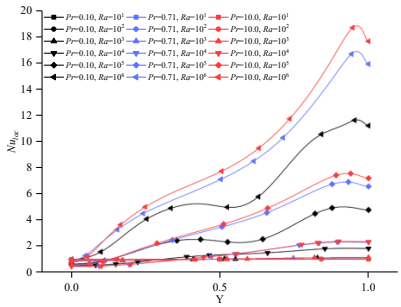
Figure S12 illustrates how the fin conductivity ratio affects the enclosure's thermal performance. As the fin conductivity ratio (k_{fin}/k) increases from 1 to 100, significant changes in local heat transfer occur for both the cold and hot walls, particularly at higher Rayleigh and Prandtl numbers.

On the cold wall, a higher k_{fin}/k ratio notably enhances the local Nusselt number distribution. With a k_{fin}/k of just 1, heat transfer remains moderate and localized, particularly at lower Rayleigh numbers where conduction dominates. In contrast, as the conductivity ratio increases to 10 and then to 100, the Nusselt number rises significantly with height, especially at Rayleigh numbers of 10^5 and 10^6. This enhancement occurs because a fin with increased thermal conductivity improves heat redistribution from hotter to colder regions of the cavity, thus intensifying convective flow and boosting thermal gradients.

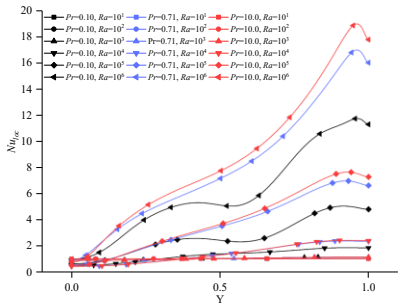
The impact of k_{fin}/k on the hot wall is notably significant but presents in a different manner. When k_{fin}/k equals 1, the Nusselt number stays fairly constant across much of the wall, exhibiting minor local peaks close to the fin. However, as conductivity increases to 10 and 100, more pronounced and localized peaks emerge near the fin base and in the upper sections of the wall. This pattern illustrates how a highly conductive fin can more effectively draw heat from the hot area and channel it into the core flow, enhancing local convective currents near the hot boundary.

It's crucial to understand that fin conductivity has a negligible effect at low Rayleigh and Prandtl numbers because pure conduction prevails. In contrast, the effect becomes significant at high Rayleigh and Prandtl conditions. For example, when $Pr = 0.71$ and $Pr = 10$ and $Ra \geq 10^4$, the fin acts as an effective thermal bridge, enhancing buoyancy-driven circulation and markedly improving heat transfer efficiency on both walls.

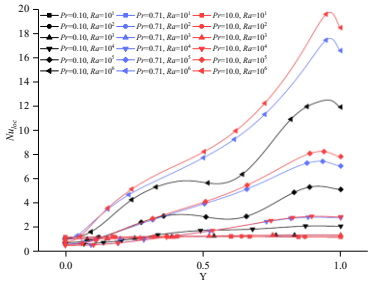
In conclusion, increased fin conductivity enhances the thermal performance of the cavity by amplifying temperature gradients and strengthening natural convection cells. This improvement is especially significant at elevated *Ra* and *Pr numbers*, where convection is the primary mechanism. Thus, choosing materials with high conductivity is crucial in fin design to optimize natural convective heat transfer within enclosures.



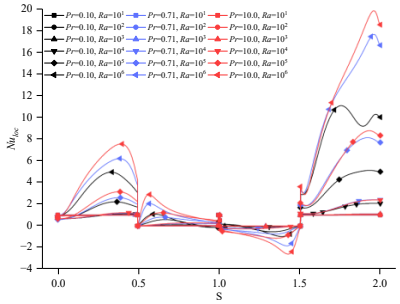
Cold wall Nu_{loc} variation for $k_{fin}/k = 1$



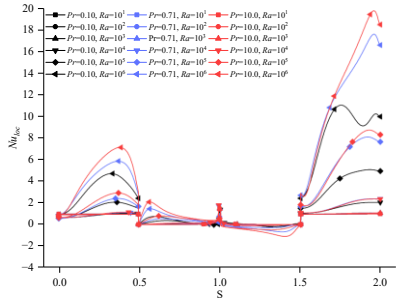
Cold wall Nu_{loc} variation for $k_{fin}/k = 10$



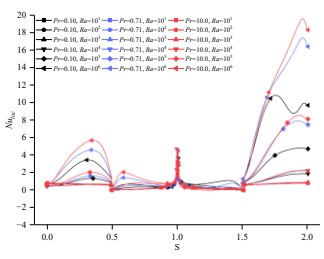
Cold wall Nu_{loc} variation for $k_{fin}/k = 100$



Hot wall Nu_{loc} variation for $k_{fin}/k = 1$



Hot wall Nu_{loc} variation for $k_{fin}/k = 10$



Hot wall Nu_{loc} variation for $k_{fin}/k = 100$

Figure S12. Variation of the Local Nusselt Number Along the Cold and Hot Walls of the Cavity for Different Conductivity Ratios (k_{fin}/k = 1, 10, and 100) at Various Rayleigh and Prandtl Numbers.

Table S5 comprehensively analyzes the Normalized Nusselt Ratio (NNR) for a square cavity with a vertical fin located at mid-height (Y_{fin} = 0.5). This study maintains a constant fin length (L_{fin} = 0.5) and fin thickness (W_{fin} = 0.01). It examines three thermal conductivity ratios (k_{fin}/k = 1, 10, and 100) in the context of laminar natural convection. Additionally, the research spans a wide range of Rayleigh numbers (Ra = 10 to 1,000,000) and Prandtl numbers (Pr = 0.1 to 10.0).

At the lowest Rayleigh number (Ra = 10), the Nusselt number ratio (NNR) stays nearly at 1 for all Prandtl numbers, provided the conductivity ratio is one (k_{fin}/k = 1). This indicates that the fin has minimal impact under weak buoyancy-driven flow. However, raising the conductivity ratio to 10 at this low-Ra results in a significant decline in NNR to approximately 0.9957 for all Pr values, and it further decreases to around 0.9494 when k_{fin}/k equals 100. This implies that fins with high conductivity enhance conductive heat redistribution along the wall, thus diminishing local convective gradients and lowering the Nusselt ratio. The maximum NNR over Pr (bold) values are almost indistinguishable across Pr, while the maximum NNR over k_{fin}/k (underlined) values show no clear preference, confirming that thermal conductivity has negligible effect in the absence of convection.

As Ra increases to 10^2 and 10^3, the same trend continues but with greater complexity. For instance, at Ra = 10^3, the NNR decreases from approximately 0.8997 at k_{fin}/k = 1 to around 0.8961 at k_{fin}/k = 10, and then further to about 0.8561 at k_{fin}/k = 100. This decline is particularly noticeable for lower Prandtl numbers (e.g., Pr = 0.1), where thermal diffusivity plays a significant role, enabling the highly conductive fin to distribute heat more evenly. This effect results in a flatter temperature gradient and diminishes the overall enhancement in heat transfer, as indicated by the Nusselt number. This trend is mirrored in the maximum NNR over Pr (bold) values, which generally fall at Pr = 10.0, and the maximum NNR over k_{fin}/k (underlined) values, which begin to favor higher conductivity ratios but with small margins.

At Ra = 10^4, a stronger response to both Pr and k_{fin}/k emerges. For Pr = 10.0, the NNR increases from 0.5978 at k_{fin}/k = 1 to 0.6397 at k_{fin}/k = 100. The rise is more pronounced with higher Pr, indicating that as thermal boundary layers become thinner, the thermal conductivity of the fin becomes increasingly important in dictating the temperature field. The maximum NNR over Pr (bold) values now consistently appear at Pr = 10.0, and the maximum NNR over k_{fin}/k (underlined) values shift toward k_{fin}/k = 100, especially at high Pr, confirming the growing benefit of thermally conductive fins in convective regimes.

At Ra = 10^5, these patterns become more prominent. For Pr = 10.0, increasing the fin conductivity ratio from 1 to 100 boosts the NNR from 0.8194 to 0.8689. The benefit is especially marked for the central fin position used here, where enhanced conduction along the fin enables better thermal coupling across the fluid domain. At moderate Pr values, the advantage is still present but less dramatic. The maximum NNR over Pr (bold) values are again concentrated at Pr = 10.0, while the maximum NNR over k_{fin}/k (underlined) values remain at kfin/k = 100 for most combinations, reinforcing the performance gains from highly conductive fins in strong natural convection flows.

At $Ra = 10^6$, the effects of k_{fin}/k become dominant. For $Pr = 10.0$, the NNR increases significantly with higher conductivity: from 0.9396 at $k_{fin}/k = 1$ to 0.9591 at $k_{fin}/k = 100$. This demonstrates that when convection is vigorous and thermal gradients are steep, the thermal conductivity of the fin is critical for maximizing heat transfer. Even for $Pr = 1.0$ or 5.0, NNR values benefit from increasing k_{fin}/k, although with a slightly lower slope. Accordingly, the maximum NNR over Pr (bold) values peak at $Pr = 10.0$, and the maximum NNR over k_{fin}/k (underlined) values clearly converge toward $k_{fin}/k = 100$ across nearly all cases, especially for $Ra \geq 10^5$.

In conclusion, the findings from **Table S5** highlight the increasing role of fin thermal conductivity as Rayleigh and Prandtl numbers rise. While the effect is negligible under conduction-dominated conditions, it becomes progressively significant in convection-dominated regimes. High Prandtl number fluids benefit the most from conductive fins due to sharper thermal gradients and thinner boundary layers. The maximum NNR over Pr (bold) values emphasize the dominance of high-Pr conditions in promoting convective performance, while the maximum NNR over k_{fin}/k (underlined) values demonstrate that highly conductive fins ($k_{fin}/k = 100$) are consistently advantageous at $Ra \geq 10^4$. These markers together identify material configurations best suited for passive enhancement in natural convection systems.

Table S5. NNR of an enclosure with a fin for different Ra and Pr numbers at three conductivity ratios (k_{fin}/k = 1, 10, and 100). Other parameters are fixed ($Y_{fin} = 0.5$, $L_{fin} = 0.5$ and $W_{fin} = 0.01$). Bold values indicate the maximum NNR across Pr for a given Ra. Underlined values indicate the maximum NNR across k_{fin}/k for a fixed (Ra, Pr) combination.

Ra	k_{fin}/k	***Pr* = 0.10**	***Pr* = 0.50**	***Pr* = 0.71**	***Pr* = 1.00**	***Pr* = 5.00**	***Pr* = 10.0**
10	1	0.999986	0.999986	0.999986	0.999986	0.999986	0.999986
	10	0.995700	0.995700	0.995700	0.995700	0.995700	0.995700
	100	0.949382	0.949382	0.949382	0.949382	0.949382	0.949382
100	1	0.998604	0.998604	0.998604	0.998604	0.998604	0.998604
	10	**0.994328**	0.994327	0.994327	0.994327	0.994326	0.994326
	100	**0.948103**	0.948093	0.948092	0.948092	0.948091	0.948091
1000	1	**0.901113**	0.899746	0.899711	0.899697	0.899696	0.899698
	10	**0.897581**	0.896137	0.896095	0.896076	0.896065	0.896066
	100	**0.858291**	0.856312	0.856220	0.856166	0.856084	0.856076
10000	1	0.590534	**0.606303**	0.603928	0.601753	0.598077	0.597843
	10	0.589745	**0.607073**	0.604726	0.602522	0.598678	0.598413
	100	0.583531	**0.610087**	0.607962	0.605642	0.600863	0.600415
100000	1	0.681382	0.789783	0.803259	0.810365	0.818652	**0.819449**
	10	0.676528	0.786376	0.799778	0.806740	0.814427	**0.815109**
	100	0.661851	0.782031	0.795806	0.802792	0.809304	**0.809638**
1000000	1	0.815091	0.887793	0.901200	0.913453	0.937712	**0.939554**
	10	0.810360	0.883628	0.896727	0.908699	0.932061	**0.933755**
	100	0.797519	0.877421	0.890102	0.901663	0.922771	**0.924137**

S5. Main Findings

The findings are supported by detailed figures, streamlines, isotherms, and tabulated Nusselt numbers provided in above. Below is a synthesis of the most significant findings derived from the parametric investigation:

5.1. Conduction-Dominated Regime ($Ra \leq 10^2$): Negligible Fin Effect

In this low-Ra regime, buoyancy-driven motion is weak or absent, and heat transfer occurs primarily by conduction. The flow field remains almost

quiescent, and the isotherms appear as vertical, undisturbed lines regardless of fin placement, shape, or fluid properties. The normalized Nusselt ratio (NNR) consistently hovers near 1.0, indicating that the fin neither enhances nor impedes heat transfer. In systems operating under weak thermal gradients or low Grashof numbers (e.g., space-constrained electronic enclosures with minimal temperature differentials), the inclusion of internal fins offers no thermal advantage and may be omitted without performance loss.

5.2. Intermediate Rayleigh Numbers ($Ra \approx 10^3$–10^5): Fin Geometry Influences Flow Symmetry and Heat Transfer

As Ra increases into the transitional convection regime, buoyancy forces begin to organize coherent circulation patterns. Here, the placement of the fin becomes critical: a mid-height position ($Y_{fin} = 0.5$) effectively splits the primary circulation cell into two symmetrical vortices, promoting uniform thermal mixing and enhancing wall heat transfer, especially for fluids with $Pr \geq 1$. Fin lengths around $L_{fin} = 0.5$ were found to be optimal for maximizing convective engagement without overextending into the flow path. For applications like passive solar collectors, natural convection heat sinks, or battery pack cooling where temperature gradients drive moderate convection, optimal fin positioning can lead to significant thermal gains without mechanical complexity.

5.3. High Rayleigh Number Regime ($Ra = 10^6$): Fin Conductivity and Position Drive Maximum Performance

The flow becomes vigorously convective at high *Ra* with thin thermal boundary layers and strong upward plume development. The interaction between fin conductivity and vertical position in this regiem determines the performance ceiling. High-conductivity fins ($k_{fin}/k = 100$) placed at $Y_{fin} = 0.5$ result in peak NNR values approaching 0.94 for $Pr = 10$ due to enhanced thermal coupling and vortex symmetry. However, fins placed too low or too high may obstruct the dominant flow path, leading to asymmetric heat transfer and reduced effectiveness. For thermally demanding enclosures (e.g., high-power electronics, LED cooling, or solar cavity receivers), selecting highly conductive fins placed at the cavity's thermal center offers the best balance of heat spreading and convective facilitation.

5.4. Geometric Sensitivity: Overly Long or Thick Fins Can Impair Convection

While increasing fin length or thickness can intuitively enhance surface area and conduction, the results show a threshold beyond which the fin becomes a hydrodynamic obstacle. Specifically, $L_{fin} > 0.5$ or $W_{fin} \geq 0.05$ begins to block the upward buoyant flow, distort recirculation, and reduce NNR values. This effect is more pronounced at high Ra, where large fin cross-sections easily disrupt narrow thermal boundary layers. Fin geometry must be optimized not only for thermal conduction but also for fluid dynamic compatibility. Designs for natural convection systems should avoid overextended or excessively thick fins that act as baffles rather than thermal bridges.

5.5. Summary of Results

The key findings from the parametric analysis have been synthesized into a summary matrix shown in **Table S6** to aid practical implementation and design decision-making. This table consolidates optimal fin configurations across a range of Rayleigh and Prandtl numbers, identifying how geometric

parameters (fin position, length, thickness) and material properties (thermal conductivity ratio) influence thermal performance. The regimes are categorized based on the relative dominance of conduction and convection and the corresponding flow behavior observed in the simulations. For each regime, design recommendations are provided to guide the selection of fin configurations that maximize heat transfer efficiency while avoiding flow obstruction or thermal stagnation. This summary is intended to serve as a practical reference for engineers and researchers designing passive thermal systems based on natural convection in enclosure-type geometries.

Table S6. Optimal fin configurations across Rayleigh and Prandtl number regimes, with dominant flow regimes and design recommendations for natural convection systems.

Parameter	$Ra \leq 10^2$	$Ra = 10^3 – 10^4$	$Ra = 10^5$	$Ra = 10^6$, $Pr \geq 5$	$Ra = 10^6$, $Pr \leq 1$
Dominant Regime	Pure conduction	Mixed conduction–weak convection	Fully developed laminar natural convection	Strong buoyancy-driven convection	Momentum-limited convection with thermal diffusion
Optimal Fin Position (Y_{fin})	Any	0.5 (mid-height)	0.5	0.5	0.3 or 0.7
Recommended Length (L_{fin})	Any	~0.5	0.3 – 0.5	~0.5	≤ 0.3
Recommended Thickness (W_{fin})	Any	~0.01	~0.01	0.01	≤ 0.01
Conductivity Ratio (k_{fin}/k)	Any	≥ 10	10 – 100	100	≥ 10
Performance Insight	Fin has a negligible effect	Enhances vortex symmetry and increases wall heat transfer	Balance between enhanced mixing and obstruction risk	Maximizes stratification and vortex strength	Mid-height fins interfere with weak plumes; off-center better
Normalized Nusselt Ratio (NNR)	≈ 1.00	~0.60–0.72	~0.80–0.87	Up to ~0.94	~0.72 – 0.90
Design Recommendation	Fin can be omitted	Avoid long or thick fins that impede weak convection	Use compact, high-k fins to enhance symmetry and performance	High-k, mid-height fin yields optimal convection	Avoid mid-height; use fins to guide or deflect plumes

As shown in **Table S6**, optimal fin design depends strongly on the balance between buoyancy strength (Rayleigh number) and fluid thermal properties (Prandtl number). In conduction-dominated regimes, fin geometry has minimal effect, while in convection-driven flows, fin placement and conductivity play critical roles in shaping flow symmetry and thermal enhancement. Mid-height, high-conductivity fins are generally preferred under strong convection, whereas off-center configurations are more effective for low-*Pr* fluids or asymmetrical flows. These trends offer practical design guidance for enhancing passive cooling in enclosure-based systems across various thermal conditions.

These findings provide a practical foundation for passive thermal management design in enclosure-type systems. For instance, electronics housings, battery compartments, and solar cavity receivers often rely on natural convection

for heat dissipation, making the optimization of internal fin geometry critical. The results suggest that placing thin, thermally conductive fins at mid-height maximizes heat transfer in high-*Ra* environments. In contrast, careful fin length and thickness adjustment can prevent flow obstruction. The summary table and NNR data herein can assist designers in selecting geometry-performance trade-offs tailored to their application's thermal regime and working fluid.

Funding: This research received no external funding.

Institutional Review Board Statement: Not applicable.

Informed Consent Statement: Not applicable.

Data Availability Statement: The data presented in this study are available on request from the corresponding author due to privacy and legal reasons.

Acknowledgments: The author gratefully acknowledges Umm Al-Qura University, Makkah, Saudi Arabia, for providing the facilities and resources that supported the successful completion of this research.

Conflicts of Interest: The author declares no conflicts of interest.

Abbreviations.

The following abbreviations are used in this manuscript:

Ra	Rayleigh Number
Pr	Prandtl Number
Nu	Nusselt Number
Nu_{loc}	Local Nusselt Number
Nu_{avg}	Average Nusselt Number
NNR	Normalized Nusselt Ratio
FEM	Finite Element Method
CFD	Computational Fluid Dynamics
FVM	Finite Volume Method
LBM	Lattice Boltzmann Method
COMSOL	COMSOL Multiphysics Software
U	Dimensionless velocity in the x-direction
V	Dimensionless velocity in the y-direction
Ψ (Psi)	Dimensionless Stream Function
θ	Dimensionless Temperature
X, Y	Dimensionless spatial coordinates
L_{fin}	Fin Length
W_{fin}	Fin Thickness
Y_{fin}	Fin Vertical Position
k_{fin}/k	Thermal Conductivity Ratio (fin to fluid)